J. Fluid Mech. (2024), *vol*. 991, A15, doi:10.1017/jfm.2024.520

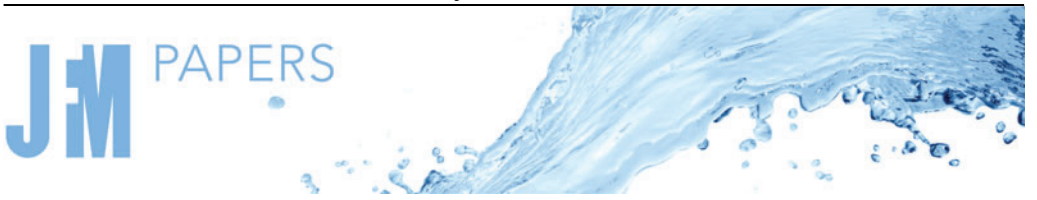

Collisionless kinetic theory for saltation over a rigid, bumpy bed

Diego Berzi[1],†, **Alexandre Valance**[2] **and James T. Jenkins**[3]

[1]Department of Civil and Environmental Engineering, Politecnico di Milano, 20133 Milano, Italy

[2]Institut de Physique de Rennes, CNRS UMR 6251, Université de Rennes I, 35042 Rennes, France

[3]School of Civil and Environmental Engineering, Cornell University, Ithaca, NY 14853, USA

(Received 9 November 2023; revised 17 May 2024; accepted 18 May 2024)

We employ the methods of statistical mechanics to obtain closures for the balance equations of momentum and fluctuation kinetic energy that govern the ballistic motion of grains rebounding at a rigid, bumpy bed that are driven by turbulent or non-turbulent shearing fluids, in the absence of mid-trajectory collisions and fluid velocity fluctuations. We obtain semi-analytical solutions for steady and fully developed saltation over horizontal beds for the vertical profiles of particle concentration and stresses and fluid and particle velocities. These compare favourably with measurements in discrete-element numerical simulations in the wide range of conditions of Earth and other planetary environments. The predictions of the particle horizontal mass flux and its scaling with the amount of particles in the system, the properties of the carrier fluid and the intensity of the shearing also agree with numerical simulations and wind-tunnel experiments.

Key words: kinetic theory, particle/fluid flow, sediment transport

1. Introduction

Saltation, that is the motion of solid particles driven by a shearing flow in a gravitational field through successive jumps and rebounds from a base driven by a shearing flow, has been established as the main mode of transport of wind-blown sand (Bagnold 1941; Owen 1964; Andreotti 2004; Charru, Andreotti & Claudin 2013; Valance *et al.* 2015) and is crucial to the dynamics of dunes (Sauermann, Kroy & Herrmann 2001). Although originally identified as the means of transport of sand grains by the wind on Earth, it has been recognized as significant also for the transport of sand or gravel in water on Earth (Fernandez Luque & Van Beek 1976; Abbott & Francis 1977; Niño & García 1998; Ancey *et al.* 2002), basalt particles on Venus (Iversen & White 1982; Greeley *et al.* 1984) and Mars (Iversen *et al.* 1976; Iversen & White 1982), and ice particles on Titan (Burr *et al.* 2015). While these studies considered the carrier fluid to be turbulent, saltation

† Email address for correspondence: diego.berzi@polimi.it

in viscous, non-turbulent fluids has also been investigated (Charru & Mouilleron-Arnould 2002; Ouriemi, Aussillous & Guazzelli 2009; Seizilles *et al.* 2014), given its practical relevance in limiting the transport capacity of oil in pipes (Dall'Acqua *et al.* 2017; Leporini *et al.* 2019).

There is a large body of mathematical models of saltation in the literature (see, e.g. the reviews of Kok *et al.* 2012; Valance *et al.* 2015; Pähtz *et al.* 2020). As highlighted by Valance *et al.* (2015), the different models can be said to be Lagrangian or Eulerian, based upon the point of view adopted in the description of the particle motion.

In many Lagrangian approaches (Anderson *et al.* 1988; Werner 1990; Creyssels *et al.* 2009; Kok & Renno 2009), particle trajectories are calculated from a distribution of the take-off velocities by solving the differential equations of their momentum balances, influenced by fluid drag and gravity, when immersed in a fluid with a prescribed velocity profile and for a given distribution of initial take-off velocity at the basal boundary. The calculation is repeated once the fluid velocity profile and the distribution of the take-off velocities are updated. This is done using a simple constitutive relation for the fluid shear stress (in the case of turbulent fluid, usually based on a mixing length approach) and a suitable set of boundary conditions that govern the impact of the particles at the base (Oger *et al.* 2005; Beladjine *et al.* 2007; Crassous, Beladjine & Valance 2007), until a steady state is attained.

Simpler Lagrangian approaches, in which the distribution of the particle trajectories is replaced by a single trajectory (Jenkins & Valance 2014) or a pair of trajectories (Andreotti 2004), have also been recently proposed and successfully compared against experiments and numerical simulations. In particular, the one trajectory models, also called periodic trajectory (PT) models, have been applied to saltation in both turbulent (Berzi, Jenkins & Valance 2016) and viscous (Pähtz *et al.* 2021; Valance & Berzi 2022) shearing flows, for values of the ratio of the grain-to-fluid mass densities encountered on Earth and other planetary bodies (Berzi, Valance & Jenkins 2017). The PT models are simple enough to allow for fully analytical solutions of steady and fully developed saltation, and permit rather accurate determination of global quantities, such as the particle mass flux, as a function of the intensity of the shearing flows. On the other hand, many variables of interest, such as the profile of the particle concentration and the total depth of the saltation layer, are poorly predicted. It is also not obvious how to extend this model to unsteady and/or inhomogeneous problems.

Another family of Lagrangian approaches is based on the framework of the discrete element method (DEM, Cundall & Strack 1979), and solves Newton's laws of motion for the individual grains that are allowed to collide with other particles and with the base, while the surrounding fluid is replaced by forces (such as drag and buoyancy) acting on the particles themselves (Tsuji, Kawaguchi & Tanaka 1993). The corresponding forces transmitted by the particles on the fluid are then introduced in the fluid momentum balance, ensuring an instantaneous two-way coupling. These discrete-continuum (DC) numerical simulations are a powerful tool, in that they greatly reduce the number of assumptions necessary to solve for the transport process. For instance, the dynamics of the impact of the particles with the base must not be modelled in advance, but is an output of the simulations. Likewise, the possibility of interparticle collisions above the base is naturally accounted for. On the other hand, the number of particles that it is feasible to simulate is severely limited by the computational power and is nowhere near to the actual number of grains involved in real-scale applications. Discrete-continuum simulations have been applied to saltation in turbulent (Durán, Andreotti & Claudin 2012; Pähtz *et al.* 2015; Pähtz & Durán 2020; Ralaiarisoa *et al.* 2020) and viscous flows (Valance & Berzi 2022)

and provide a large number of measurements, some of which are simply unattainable in physical experiments. Hence, they serve as severe tests of more sophisticated approaches.

Eulerian approaches, in which both the fluid and the saltating particles are treated as two superimposed continuum phases, offer the most promising perspective for modelling large-scale phenomena. In the model of Sauermann *et al.* (2001), the motion of the two phases is depth averaged over the saltation layer, and cannot therefore predict the distribution of the variables of interest with height. A key point of the model is that the wind profile in the saltation layer is determined by assuming an exponential distribution of the particle shear stress there. The same assumption is adopted in more recent Eulerian models (Lämmel, Rings & Kroy 2012; Pähtz, Kok & Herrmann 2012). Assuming an *a priori* distribution of velocity is crucially different from phrasing a constitutive relation for the particle shear stress, and obtaining the distribution from the usual momentum balance.

Pasini & Jenkins (2005) were the first to average the equations governing the trajectory of the single particles to obtain boundary conditions for collisional saltation. Later, Jenkins, Cantat & Valance (2010) proposed a constitutive relation for the particle shear stress based on substituting averaging of products with products of averaging. They also equated the particle pressure to the product of the particle concentration and the granular temperature, the mean square of the particle velocity fluctuations. They assumed, as in Creyssels *et al.* (2009), that the latter is uniformly distributed with the distance from the base, which holds only if the vertical drag on the particles is negligible. From the uniform distribution of the granular temperature, they obtained the exponential decay of the particle concentration and distributions of particle and fluid mean horizontal velocities that agreed reasonably well with experiments (Creyssels *et al.* 2009; Chassagne, Bonamy & Chauchat 2023). The model was later extended to deal with unsteadiness and inhomogeneities (Jenkins & Valance 2018). Interestingly, the constitutive relation for the particle shear stress of Jenkins *et al.* (2010) coincides with the dilute and collisionless limit of the expression derived by Garzó *et al.* (2012) by solving the Enskog kinetic theory for monodisperse gas–solid flows, as already pointed out in Chassagne *et al.* (2023). However, in the present context, such a relation for the particle shear stress is too simple in that it ignores a contribution from the difference in velocities and results from assuming that the vertical particle velocity fluctuations are not influenced by drag (Jenkins *et al.* 2010; Jenkins & Valance 2014) or are distributed isotropically (Garzó *et al.* 2012).

Here, our goal is to employ a kinetic theory that includes drag, gravity and a distribution of particle velocities to obtain continuum expressions for the stresses and energy flux in a collisionless flow of particles in shearing flows of a general fluid above a horizontal, rigid, bumpy boundary. Such a boundary is particularly effective in transferring momentum from the horizontal to the vertical. As a consequence, in a steady, uniform flow, the vertical component of the velocity after a collision is likely to be larger than the particle settling velocity. We distinguish between ascending and descending particles, approximate the trajectories based on the characteristics of a rigid bumpy boundary in the limit of large vertical velocity of the ascending particles with respect to the settling velocity, and assume that the velocity distribution function of the ascending particles is an anisotropic Maxwellian, as in Creyssels *et al.* (2009). In this case, the second velocity moment of the distribution is a second-rank tensor, rather than a scalar. Also, it is assumed that, at each position above the bed, the fluid velocity profile, when expanded at that position, is linear for viscous flows and logarithmic for turbulent flows. Averaging, then, permits approximate analytical forms to be obtained for the particle stresses and energy flux in both viscous and turbulent flows.

As suggested by Pasini & Jenkins (2005), collisions above the base can be ignored if the mean free path of kinetic theory is larger than the length of the ballistic trajectory. Given that the mean free path strongly decreases if the particle concentration increases (Chapman & Cowling 1970), and that the particle concentration near erodible beds that are composed of particles at rest identical to those in saltation is large (Tholen *et al.* 2023), we argue that collisionless saltation is possible only over a rigid bed.

We phrase and solve the balances of fluid and particle momenta and particle fluctuation energy for steady, fully developed saltation over a horizontal, rigid, bumpy bed, driven by either a viscous or turbulent shearing flow, using the boundary layer approximation for the fluid flow, with appropriate boundary conditions. As in all previous models of saltation, we assume that the fluid velocity is solely in the horizontal direction and neglect its fluctuations. This permits us to uncouple the determination of quantities associated with the particle vertical motion, such as the intensity of the vertical velocity fluctuations, particle concentration and normal stress, from those that involve the particle horizontal motion and are, therefore affected by the flow regime of the fluid, such as the particle shear stress and particle and fluid mean horizontal velocity. Depending on the flow regime of the fluid, only one or two differential equations must be solved numerically to determine the vertical profiles of the corresponding quantities. The remainder of the profiles, including the depth of the saltation layer, are obtained algebraically.

After deriving scaling laws for flow quantities in some special limits, we successfully test the results of the theory against quasi-two-dimensional DC simulations of saltation in viscous and turbulent shearing flows. These were carried out by suppressing the possibility of mid-trajectory collisions for a wide range of particle-to-fluid mass density ratios, ranging from Mars to Earth, at different values of the strength of the shearing flows, the amount of particles in the system and the viscosity of the fluid. We also test the relation between the particle mass flux and the amount of particles in the system against measurements made in wind-tunnel experiments (Ho 2012).

In § 2, we present the constitutive relations, the balance equations and the boundary conditions that we employ to obtain semi-analytical solutions to steady and fully developed saltation over rigid, bumpy beds. In § 3, we show how to obtain scaling laws for various quantities in the limit of rarefied saltation in both viscous and turbulent flows, at least when the drag coefficient reduces to its asymptotic expressions. Comparisons against DC simulations and experiments are detailed in § 4. Finally, in § 5, we conclude with a summary of the main findings and an outline of future work.

2. Governing equations and semi-analytical solutions

The saltating particles are assumed to be identical spheres of diameter d and mass density ρ^s. A shearing flow of a fluid of mass density ρ^f and molecular viscosity μ^f drives the flow in the presence of gravity, with g the gravitational acceleration. The mean horizontal velocities of the particles and the fluid are u and U, respectively. We assume that the flow is steady and uniform, so that the velocities are only functions of the vertical distance from the bed y. We imagine that the bed is made bumpy by gluing identical particles of diameter d_w, in close contact to each other, over a flat plate. Hence, the ratio of d_w to d is a natural measure of the bed roughness. We characterize the particles through the fall particle Reynolds number $R = \rho^f \sqrt{g(r-1)/r} d^{3/2}/\mu^f$, where $r = \rho^s/\rho^f$ is the density ratio. A sketch of the flow configuration is shown in figure 1. In what follows, all quantities are made dimensionless using the diameter and mass density of the particles and the reduced gravitational acceleration, $g(r-1)/r$. Then, lengths, velocities and stresses are expressed in units of d, $[g(r-1)d/r]^{1/2}$ and $\rho^s g(r-1)d/r$, respectively.

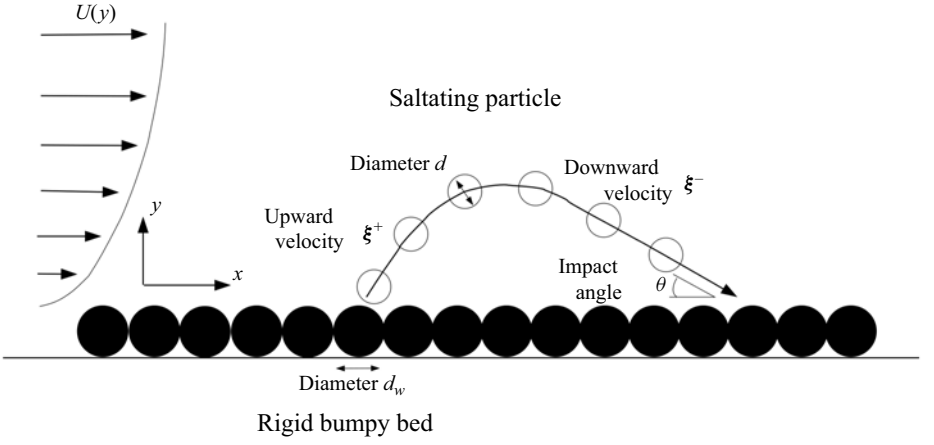

Figure 1. Sketch of a particle driven into saltation over a rigid, bumpy bed by a shearing flow.

The balance equations for the y and x-momenta of the particles, under steady and fully developed conditions, are, respectively,

$$\frac{\mathrm{d}\sigma_y}{\mathrm{d}y} = -c; \tag{2.1}$$

and

$$\frac{\mathrm{d}s}{\mathrm{d}y} = -cC_D(U-u), \tag{2.2}$$

where σ_y and s are the particle normal stress in the y-direction and the particle shear stress, respectively; c is the particle volume concentration; and C_D is the drag coefficient that, for a single particle, has a component independent of the relative velocity between the single particle and the fluid and a component proportional to the absolute value of that velocity difference. Here, we assume perhaps the simplest form of C_D (Dallavalle 1943), which we make independent of y by evaluating it at the bed in the case of saltation in viscous flows,

$$C_D = \frac{18}{St} + \frac{0.3}{r}|U_0 - u_0|, \tag{2.3a}$$

where $St = rR$ is the fall Stokes number and the subscript 0 indicates quantities evaluated at the bed. We employ the terms Stokes drag to refer to situations in which $C_D \simeq 18/St$, form drag for situations in which $C_D \simeq 0.3|U_0 - u_0|/r$ and nonlinear drag for the generic case in which both Stokes and form drag are present. A more appropriate expression for the average C_D should also involve the strength of the particle velocity fluctuations (Jenkins & Hanes 1998). However, including it would have only a small quantitative effect on the results. Also permitting the drag coefficient to vary along y does not significantly alter the solution to the continuum model. We anticipate that, while (2.3a) works well for saltation in viscous shearing flows over rigid, bumpy beds, where the fluid and particle velocity profiles are approximately linear, a more appropriate expression for saltation in turbulent flows should incorporate the difference in the concentration-weighted average velocities between the two phases, as proposed by Pähtz *et al.* (2021)

$$C_D = \frac{18}{St} + \frac{0.3}{r}|\bar{U} - \bar{u}|, \tag{2.3b}$$

where $\bar{U} - \bar{u} = \int_0^h c(U-u)\,\mathrm{d}y / \int_0^h c\,\mathrm{d}y$, with h the depth of the saltation layer.

For flows over rigid beds, we take the no-slip boundary condition for the fluid

$$U_0 = 0. \tag{2.4}$$

If saltating particles with a large value of the coefficient of sliding friction impact a rigid, bumpy bed at a small mean angle θ with respect to the horizontal (figure 1), then, using the analysis of Lämmel *et al.* (2017) in Appendix C,

$$u_0 = \alpha_u \frac{1}{C_D \theta}, \tag{2.5}$$

where α_u is a strictly positive coefficient of order unity that is weakly dependent on the rebound properties of the particles and the flow regime of the fluid. The reason for the latter dependence is that the probability distributions of impact angles are qualitatively different for saltation in viscous and turbulent shearing flows (Appendix C).

In a steady, uniform flow, in the absence of a horizontal pressure gradient, the sum of the fluid and particle shear stress, S and s, respectively, is constant and equal to the far-field fluid shear stress, which, in dimensionless terms, is the Shields parameter

$$s + S = Sh. \tag{2.6}$$

To close the problem, we require constitutive relations for the particle and fluid stresses.

In the absence of particle collisions above the bed, the only mechanism responsible for the particle stresses is the transfer of momentum associated with the particles crossing a reference surface. Hence, the particle normal stress in the y-direction is simply given by the average vertical flux of y-momentum

$$\sigma_y = cT_y, \tag{2.7}$$

where T_y is the mean square of the vertical velocity fluctuations of the particles . There is a corresponding mean square of the horizontal velocity fluctuations T_x, where T_x and T_y are the diagonal components of the second moment of the particle velocity tensor.

The distribution of the additional hydrodynamic field, T_y, along y is governed by the balance of kinetic energy associated with the particle vertical motion, that is, the yy-component of the particle second-moment tensor, which, in a steady and fully developed flow, and in the absence of mid-trajectory collisions and fluid velocity fluctuations, reduces to (Saha & Alam 2016, 2017)

$$-\frac{\mathrm{d}Q_{yyy}}{\mathrm{d}y} - 2C_D\sigma_y = 0. \tag{2.8}$$

Here, Q_{yyy} is the y-component of the flux of the kinetic energy associated with the vertical particle velocity fluctuations and $2C_D\sigma_y$ is its dissipation due to the fluid drag.

Assuming that the fluid motion is only horizontal and that the drag coefficient is independent of y, we can obtain approximate analytical expressions for the trajectories of the saltating particles even in the turbulent case (Appendix A). In doing so, we distinguish between ascending and descending particles. Then, the horizontal, ξ_x^-, and vertical, ξ_y^-, velocities of any descending particle at a given distance y from the bed can be obtained analytically from the horizontal, ξ_x^+, and vertical, ξ_y^+, velocities of the same particle at the same distance y from the bed during its ascending motion. In the classical framework of statistical mechanics, we introduce a velocity distribution function, f^+, for the ascending particles, so that $(\pi/6)\int_{all\ \xi^+} f^+ \,\mathrm{d}^2\boldsymbol{\xi}^+$ gives the concentration of the ascending particles. With this, $Q_{yyy} = (\pi/6)\int_{all\ \xi^+} (\xi_y^{+2} - \xi_y^{-2})\xi_y^+ f^+ \,\mathrm{d}^2\boldsymbol{\xi}^+$. With the further assumptions that

the velocity distribution function is an anisotropic Maxwellian (Creyssels *et al.* 2009) and that the vertical velocity ξ_y^+ of the ascending particles is much larger than $1/C_D$ (the settling velocity), we derive a simple expression for Q_{yyy} in Appendix B

$$Q_{yyy} = \sqrt{\frac{8}{\pi}} c^+ (T_y^+)^{3/2}. \tag{2.9}$$

Here, c^+ and T_y^+ are the volume concentration and the mean square of the vertical velocity fluctuations of the ascending particles, respectively. In a steady state, c^+ and T_y^+ are related to c and T_y through (see Appendix B)

$$c = c^+ \left(2 + \frac{3}{4} C_D \sqrt{\frac{2T_y^+}{\pi}} \right); \tag{2.10}$$

and

$$T_y = \frac{4\sqrt{\pi} C_D T_y^+ + 4\sqrt{2T_y^+}}{8\sqrt{\pi} C_D + 3C_D^2 \sqrt{2T_y^+}}. \tag{2.11}$$

As explicitly shown in Appendix B, the assumption that the vertical velocity of the ascending particles is much larger than the settling velocity is a good approximation for $C_D\sqrt{T_y} > 1$. We will see in § 4 that this condition is not satisfied only near the top of the saltation layer.

Using (2.7), (2.10) and (2.11) into (2.1) leads to

$$\frac{\mathrm{d}c^+}{\mathrm{d}y} = -c^+ \frac{8C_D + 3C_D^2\sqrt{2T_y^+/\pi}}{4C_D T_y^+ + 4\sqrt{2T_y^+/\pi}} - c^+ \frac{2C_D + \sqrt{2/\pi T_y^+}}{2C_D T_y^+ + 2\sqrt{2T_y^+/\pi}} \frac{\mathrm{d}T_y^+}{\mathrm{d}y}, \tag{2.12}$$

that, combined with (2.8) and (2.9), permits an ordinary differential equation for T_y^+ to be obtained

$$[\sqrt{8\pi} C_D (T_y^+)^{3/2} + 8T_y^+] \frac{\mathrm{d}T_y^+}{\mathrm{d}y} = (6 - 4\pi) C_D^2 (T_y^+)^2 - 8T_y^+. \tag{2.13}$$

The analytical solution of this, with the boundary condition $T_y^+(y = 0) = T_{y,0}^+$, for the vertical particle velocity fluctuations at the rigid boundary, is

$$\begin{aligned} &4\sqrt{2\pi(2\pi - 3)} \tan^{-1}\left(\frac{\sqrt{2\pi - 3}}{2} C_D \sqrt{T_y^+} \right) \\ &\quad - 2(2\pi - 3)\left\{ \sqrt{2\pi} C_D \sqrt{T_y^+} + 2\log[4 + (2\pi - 3) C_D^2 T_y^+] \right\} \\ &= (3 - 2\pi)^2 C_D^2 y + 4\sqrt{2\pi(2\pi - 3)} \tan^{-1}\left(\frac{\sqrt{2\pi - 3}}{2} C_D \sqrt{T_{y,0}^+} \right) \\ &\quad - 2(2\pi - 3)\left\{ \sqrt{2\pi} C_D \sqrt{T_{y,0}^+} + 2\log[4 + (2\pi - 3) C_D^2 T_{y,0}^+] \right\}. \end{aligned} \tag{2.14}$$

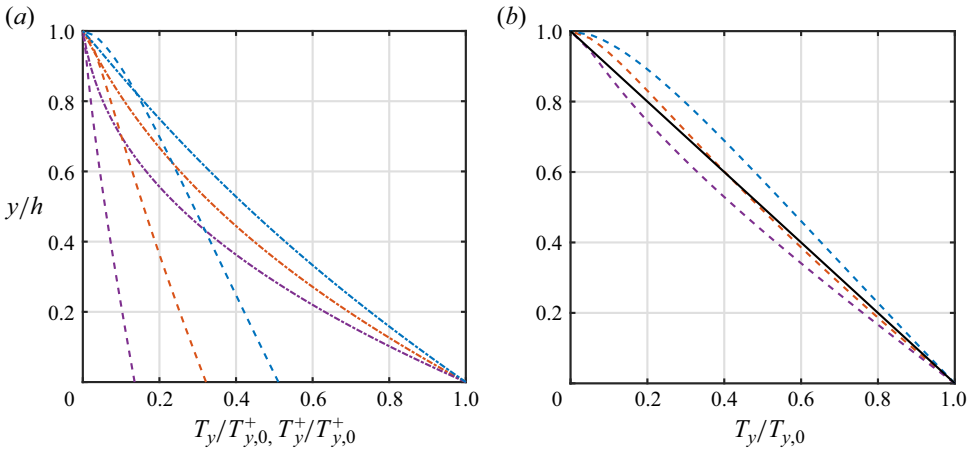

Figure 2. (*a*) Normalized profiles of T_y^+ (dot-dashed lines) and T_y (dashed lines) obtained from (2.14) and (2.11), respectively, when $C_D^2 T_{y,0}^+ = 2.5$ (blue lines), $C_D^2 T_{y,0}^+ = 10$ (orange lines) and $C_D^2 T_{y,0}^+ = 100$ (purple lines). (*b*) Normalized profiles of T_y (dashed lines, same colour legend of figure 2*a*) and the linear distribution of (2.16) (solid black line).

The non-zero value of $T_{y,0}^+$ is associated with the rebound velocity of the particles at a rigid, bumpy bed.

Under the same assumptions that were employed to derive equation (2.5), a simple dependence of $T_{y,0}^+$ calculated at the bed on the impact angle θ is obtained in Appendix C

$$T_{y,0}^+ = \alpha_T \frac{1}{C_D^2 \theta} \frac{2d_w}{1+d_w}, \tag{2.15}$$

where α_T is another strictly positive coefficient of order unity that is weakly dependent on the rebound properties of the particles and the flow regime of the fluid. We emphasize that the impact angle, and consequently $T_{y,0}^+$, remains an unknown at this stage of the analysis. We will determine it in the next two sub-sections, when we describe quantities associated with the horizontal motion of the particles that are influenced by the flow regime of the fluid.

Equation (2.14) provides the analytical distribution of T_y^+ along y, which, when employed in (2.11), gives the analytical distribution of T_y shown in figure 2(*a*) for different values of $C_D\sqrt{T_{y,0}^+}$, corresponding to an impact angle θ in (2.15) in the range 1° to 20°. As shown in figure 2(*b*), the distribution of T_y is roughly linear and well approximated as

$$T_y = \frac{h-y}{h} T_{y,0}, \tag{2.16}$$

where the depth of the saltation layer, h, is to be determined. The mean square of the particle velocity fluctuations at the bed, $T_{y,0}$, can be obtained from (2.11), when $T_{y,0}^+$ is known.

Inserting (2.7) into (2.1), with (2.16), and integrating gives the following power-law distribution of the particle concentration:

$$c = c_0\left(\frac{h-y}{h}\right)^{(h-T_{y,0})/T_{y,0}}, \tag{2.17}$$

where c_0 is the particle concentration at the bed. Integrating equation (2.1) with (2.17) also gives

$$\sigma_y = c_0 T_{y,0}\left(\frac{h-y}{h}\right)^{h/T_{y,0}}. \tag{2.18}$$

Upon introducing the hold-up, $M = \int_0^h c\,\mathrm{d}y$, i.e. the particle mass per unit basal area, by integrating the concentration through the saltation layer, with $\sigma_y = 0$ at $y = h$, we obtain

$$c_0 = \frac{M}{T_{y,0}}. \tag{2.19}$$

Integrating the energy balance, (2.8) with (2.18) and (2.19), provides

$$Q_{yyy} = 2C_D M T_{y,0}\frac{h}{h+T_{y,0}}\left[\left(\frac{h-y}{h}\right)^{(h+T_{y,0})/T_{y,0}} - 1\right] + Q_{yyy,0}, \tag{2.20}$$

where the value of Q_{yyy} at the bed can be obtained from the ratio of (2.9) and (2.7), with (2.10), (2.11) and (2.19), as

$$Q_{yyy,0} = \frac{4C_D T_{y,0}^{+}}{C_D\sqrt{2\pi T_{y,0}^{+}} + 2}M. \tag{2.21}$$

Given that Q_{yyy} must vanish at the top of the saltation layer, the depth h of the saltation layer is determined from (2.20) as

$$h = \frac{Q_{yyy,0}}{2C_D M T_{y,0} - Q_{yyy,0}}T_{y,0}. \tag{2.22}$$

The governing equations, constitutive relations and analytical results described so far apply to saltation in both viscous and in turbulent shearing flows and can be calculated only after the determination of the impact angle θ, required in (2.5) and (2.15). To proceed, we must distinguish between the two regimes of the fluid shearing flow.

Before doing that, we support the assumption that particle collisions above the bed can be neglected. As suggested by Pasini & Jenkins (2005), chances of mid-trajectory collisions are low if the mean free path, λ, the average distance travelled by a particle in between two successive collisions predicted by the kinetic theory of granular gases, is less than twice the height of the particle trajectory, here determined by gravity and fluid drag. If we use the expression for the mean free path in a dilute gas of Chapman & Cowling (1970), evaluate this at the bed and take h as the average height of the particle trajectories, we obtain

$$\lambda_0 = \frac{1}{6c_0\sqrt{2}} \geq 2h. \tag{2.23}$$

Equation (2.23), used with (2.22), implies that, for given values of r, St and Sh, there is a maximum hold-up above which mid-trajectory collisions play a role. That is, because

the mean free path is a decreasing function of the particle concentration, as the hold-up increases, collisions become more likely. However, there is also a limiting hold-up at which particles begin to deposit on the bed. Analysis of periodic trajectories over rigid beds (Jenkins & Valance 2014) and discrete simulations of the present paper indicate that the concentration at the bed at which deposition begins is greater than that at which collisions begin to occur. Consequently, in saltation over such beds, collisions occur before deposition.

2.1. *Saltation in viscous shearing flows*

In the absence of turbulence, the expression for the fluid shear stress is (Valance & Berzi 2022)

$$S = \frac{1 - c}{St}\frac{\mathrm{d}U}{\mathrm{d}y} \simeq \frac{1}{St}\frac{\mathrm{d}U}{\mathrm{d}y}, \tag{2.24}$$

where we have neglected the particle concentration with respect to unity. Equation (2.24) implies that, in the absence of particles and in the boundary layer approximation that we have employed, the fluid velocity distribution would be linear.

Using statistical mechanics arguments, the particle shear stress can be obtained as $s = -(\pi/6)\int_{all\ \xi^+}(\xi_x^+ - \xi_x^-)\xi_y^+ f^+\,\mathrm{d}^2\boldsymbol{\xi}^+$. To determine ξ_x^-, we assume in Appendix A that the fluid velocity profile encountered by an ascending particle during its ballistic trajectory above a certain position y is locally linear; that is, it is linear in the region between y and the top of the trajectory. However, the slope of the linear profile changes with y due to the drag of the particles. This assumption and the assumptions on the form of the velocity distribution function f^+ and $C_D\xi_y^+ \gg 1$, that we have already employed in the derivation of the expression for Q_{yyy} in (2.9), permit the derivation in Appendix B of a simple expression for the particle shear stress

$$s = \frac{3}{5}C_D\sigma_y\left(U - u + \frac{2}{3}\frac{1}{C_D^2}\frac{\mathrm{d}U}{\mathrm{d}y}\right). \tag{2.25}$$

Interestingly, the particle shear stress does not depend on the particle shear rate, as in Jenkins *et al.* (2010), but only on the velocity difference and on the fluid shear rate. The physical reason is that the particles do not interact with each other, but only with the surrounding fluid.

As explained in Appendix C, for saltation in viscous flows the mean angle θ between the particle velocity and the horizontal before the impact with the bed is estimated in the limit of large vertical velocity of ascending particles in Appendix A as

$$\theta = \frac{C_D}{St(Sh - s_0)}, \tag{2.26}$$

where s_0 is the particle shear stress at the bed.

Using (2.4) and (2.5) in (2.3*a*), with (2.26), we obtain a relationship between the drag coefficient and the particle shear stress at the bed

$$C_D^3 = \frac{18}{St}C_D^2 + \frac{0.3}{r}\alpha_u St(Sh - s_0). \tag{2.27}$$

The particle shear stress at the bed is obtained from (2.25), with (2.4)–(2.6), (2.19) and (2.24), as

$$s_0 = \frac{(2 - 3\alpha_u)MStSh}{5C_D + (2 - 3\alpha_u)MSt}. \tag{2.28}$$

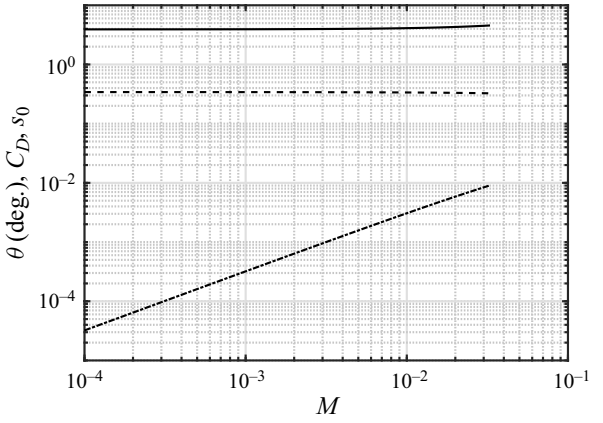

Figure 3. Predicted impact angle in degrees (solid line, –), drag coefficient (dashed line, --) and particle shear stress at the bed (dot-dashed line, ·-) as functions of the hold-up for saltation in viscous shearing flows when $d_w = 1$, $St = 100$, $r = 50$, and $Sh = 0.05$ (with $\alpha_u = 0.60$).

Equation (2.28) implies that for the particle shear stress at the bed to be positive, α_u must be less than 2/3. The system of (2.27) and (2.28) can be solved to determine the drag coefficient and the particle shear stress at the bed once the values of d_w, r, St, Sh and M are given. Then, the impact angle (2.26), the values of all the variables at the bed ((2.5), (2.15) and (2.21)), the depth of the saltation layer (2.22), and the analytical distributions of T_y^+, T_y, c, σ_y and Q_{yyy} ((2.14), (2.16)–(2.18) and (2.20)) can also be calculated for saltation in viscous shearing flows.

Figure 3 shows the variation of the impact angle, the drag coefficient and the particle shear stress at the bed with the particle hold-up, as predicted by ((2.26)–(2.28)), for, e.g. saltation of 100 μm basalt grains in viscous shearing flows on Venus, assuming that $\alpha_u = 0.60$ (§ 4 provides more details on the choice of the parameters). Equation (2.23) is satisfied for the range of hold-up in figure 3. Notice that for almost the entire range of hold-up, the particle shear stress at the bed increases linearly with M, while θ and C_D are constant.

Using (2.25) in (2.2), with (2.6), (2.18) and (2.24), gives a first-order, linear, non-homogeneous, differential equation for the particle shear stress

$$\frac{\mathrm{d}s}{\mathrm{d}y} = -\left[\frac{5}{3}\frac{1}{T_{y,0}}\left(\frac{h-y}{h}\right)^{-1} + \frac{2}{3}\frac{c_0 St}{C_D}\left(\frac{h-y}{h}\right)^{(h-T_{y,0})/T_{y,0}}\right]s + \frac{2}{3}\frac{c_0 StSh}{C_D}\left(\frac{h-y}{h}\right)^{(h-T_{y,0})/T_{y,0}}. \tag{2.29}$$

The analytical solution of (2.29) is

$$s = Sh\left(\frac{2}{3}\frac{MSt}{C_D}\right)^{5/3}\Gamma\left[-\frac{2}{3}, \frac{2}{3}\frac{MSt}{C_D}\left(\frac{h-y}{h}\right)^{h/T_{y,0}}\right] \times \exp\left\{\ln\left[\left(\frac{h-y}{h}\right)^{(5/3)(h/T_{y,0})}\right] + \frac{2}{3}\frac{MSt}{C_D}\left(\frac{h-y}{h}\right)^{h/T_{y,0}}\right\} - Sh\left(\frac{2}{3}\frac{MSt}{C_D}\right)^{5/3}\Gamma\left[-\frac{2}{3}, \frac{2}{3}\frac{MSt}{C_D}\right]$$

$$\times \exp\left\{\ln\left[\left(\frac{h-y}{h}\right)^{(5/3)(h/T_{y,0})}\right] + \frac{2}{3}\frac{MSt}{C_D}\left(\frac{h-y}{h}\right)^{h/T_{y,0}}\right\}$$
$$+ s_0 \exp\left\{\ln\left[\left(\frac{h-y}{h}\right)^{(5/3)(h/T_{y,0})}\right] + \frac{2}{3}\frac{MSt}{C_D}\left(\frac{h-y}{h}\right)^{h/T_{y,0}} - \frac{2}{3}\frac{MSt}{C_D}\right\}, \quad (2.30)$$

in which $\Gamma(s,x) \equiv \int_x^\infty t^{s-1}\, e^{-t}\, \mathrm{d}t$ is the upper incomplete gamma function.

The fluid velocity profile is determined by integrating the constitutive relation (2.24) $\mathrm{d}U/\mathrm{d}y = St(Sh - s)$, with the particle shear stress given by (2.30). Unfortunately, there is no general analytical solution. Hence, we obtain the distribution of U by numerically solving this ordinary differential equation, with the no-slip condition, (2.4), at the bed. Once U is determined, the particle horizontal velocity is given by (2.25) as

$$u = U - \frac{5}{3}\frac{s}{C_D\sigma_y} + \frac{2}{3}\frac{St(Sh-s)}{C_D^2}. \quad (2.31)$$

We can now calculate the particle flux q per unit basal area through numerical integration as

$$q = \int_0^h cu\,\mathrm{d}y. \quad (2.32)$$

In the special case of rarefied saltation, that is for $M \to 0$ and $Sh \gg s$, the analytical solution of (2.29) simplifies to

$$s = s_0\left(\frac{h-y}{h}\right)^{(5/3)(h/T_{y,0})} + \frac{MStSh}{C_D}\left[\left(\frac{h-y}{h}\right)^{h/T_{y,0}} - \left(\frac{h-y}{h}\right)^{(5/3)(h/T_{y,0})}\right], \quad (2.33)$$

and the fluid velocity profile is simply

$$U = (StSh)y. \quad (2.34)$$

Then, from (2.18), (2.28), (2.31), (2.33) and (2.34), the particle horizontal velocity is

$$u = \left[(1+\alpha_u)\left(\frac{h-y}{h}\right)^{(2/3)(h/T_{y,0})} + C_D^2 y - 1\right]\frac{StSh}{C_D^2}. \quad (2.35)$$

Notice that, in the rarefied limit of saltation in viscous shearing flows, the particle and the fluid velocity profiles are independent of the hold-up. Using (2.17), (2.19) and (2.35) in (2.32), and integrating, gives the particle flux as

$$q = MStShT_{y,0}\frac{h}{h+T_{y,0}}. \quad (2.36)$$

The above equations permit the determination of profiles of particle concentration, particle and fluid velocities and particle and fluid stresses in viscous shearing flow that will be compared with the results of DC numerical simulations in § 4.

2.2. *Saltation in turbulent shearing flows*

In the case of saltation in turbulent shearing flows, we model the fluid shear stress using the classical mixing length approach (Jenkins *et al.* 2010)

$$S = \frac{1-c}{r}\kappa^2(y+y_0)^2\left(\frac{\mathrm{d}U}{\mathrm{d}y}\right)^2 \simeq \frac{\kappa^2(y+y_0)^2}{r}\left(\frac{\mathrm{d}U}{\mathrm{d}y}\right)^2, \tag{2.37}$$

where $\kappa = 0.41$ is von Kármán's constant and $y_0 = \sqrt{r/Sh}/(9St) + (k_s/30)[1 - \exp(-k_s St\sqrt{Sh/r}/26)]$ is an empirical expression for the origin of the logarithmic fluid velocity profile that encompasses hydrodynamically smooth, rough and transitional beds (Guo & Julien 2007). The roughness length scale k_s is taken to be equal to d_w (Ho 2012).

Equation (2.37) implies that, in the absence of particles and in the boundary layer approximation that we have employed, the fluid velocity distribution would be logarithmic. We assume, as in Pähtz *et al.* (2021), that the fluid velocity profile encountered by an ascending particle during its ballistic trajectory is logarithmic even if other particles are present. This assumption, and the assumptions that we have already employed in the derivation of the expression for Q_{yyy}, (2.9), permits the derivation in Appendix B of an expression for the particle shear stress, $s = -(\pi/6)\int_{all\ \xi^+}(\xi_x^+ - \xi_x^-)\xi_y^+ f^+\,\mathrm{d}^2\xi^+$

$$s = \frac{3}{5}C_D\sigma_y\left\{U - u - \frac{\sqrt{rS}}{\kappa}\exp\left[C_D^2\frac{\sqrt{rS}}{\kappa}\left(\frac{\mathrm{d}U}{\mathrm{d}y}\right)^{-1}\right]Ei\left[-C_D^2\frac{\sqrt{rS}}{\kappa}\left(\frac{\mathrm{d}U}{\mathrm{d}y}\right)^{-1}\right]\right\}, \tag{2.38}$$

in which $Ei(x) \equiv -\int_{-x}^{\infty} e^{-t}t^{-1}\,\mathrm{d}t$ is the exponential integral. As in the viscous case of (2.25), the particle shear stress in turbulent shearing flows does not depend on the particle shear rate. The saltating particles, when treated as a continuous medium, can experience shear stress even if the horizontal particle velocity is uniform across the flow domain.

As explained in Appendix C, the mean impact angle θ for saltation in turbulent flows in the limit of large vertical velocity of ascending particles is estimated as

$$\theta \simeq -\left[C_D\frac{\sqrt{r(Sh - s_0)}}{\kappa}\exp(C_D^2 y_0)Ei(-C_D^2 y_0)\right]^{-1}. \tag{2.39}$$

Integrating equation (2.2) between $y = 0$ and $y = h$, with vanishing particle shear stress at the top of the saltation layer gives $s_0 = MC_D(\bar{U} - \bar{u})$ (Pähtz *et al.* 2021). Using this in (2.3*b*) gives the drag coefficient in terms of the particle shear stress at the bed

$$C_D = \frac{9}{St} + \sqrt{\frac{81}{St^2} + \frac{0.3}{r}\frac{s_0}{M}}. \tag{2.40}$$

Equation (2.38) evaluated at the bed, with (2.5) and (2.39) gives the particle shear stress at the bed as a function of the impact angle

$$s_0 = \frac{3}{5}\frac{M}{\theta}(1 - \alpha_u). \tag{2.41}$$

Equation (2.41) implies that, for the particle shear stress at the bed to be positive, α_u must be less than 1. Then, (2.39) with (2.40) and (2.41) results in an implicit equation for θ

$$\frac{1}{\theta}\left(\frac{9}{St} + \sqrt{\frac{81}{St^2} + \frac{0.9}{5r}\frac{1-\alpha_u}{\theta}}\right)^{-1} \simeq -\frac{1}{\kappa}\sqrt{r\left(Sh - \frac{3M}{5}\frac{1-\alpha_u}{\theta}\right)}$$

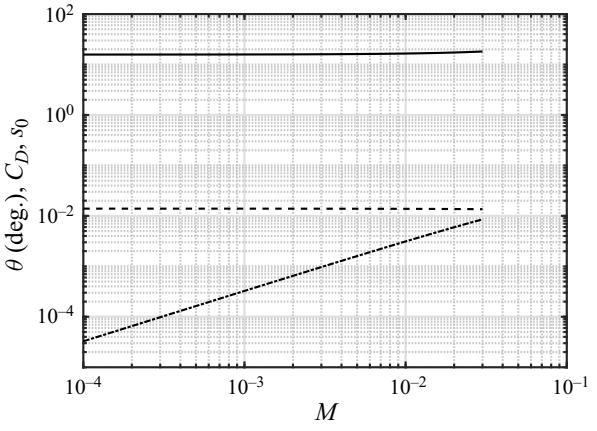

Figure 4. Predicted impact angle in degrees (solid line, –), drag coefficient (dashed line, --) and particle shear stress at the bed (dot-dashed line, ·-) as functions of the hold-up for saltation in turbulent shearing flows with $d_w = 1.5$, $St = 1681$, $r = 2208$ and $Sh = 0.04$ (with $\alpha_u = 0.85$).

$$\times \exp\left[\left(\frac{9}{St}+\sqrt{\frac{81}{St^2}+\frac{0.9}{5r}\frac{1-\alpha_u}{\theta}}\right)^2 y_0\right]$$
$$\times Ei\left[-\left(\frac{9}{St}+\sqrt{\frac{81}{St^2}+\frac{0.9}{5r}\frac{1-\alpha_u}{\theta}}\right)^2 y_0\right]. \quad (2.42)$$

This can be solved to determine the impact angle. Once θ is known, s_0 (2.41), C_D (2.40), the boundary values of the remaining variables at the bed ((2.5), (2.15) and (2.21)), the depth of the saltation layer (2.22), and the analytical distributions of T_y^+, T_y, c, σ_y and Q_{yyy} ((2.14), (2.16)–(2.18) and (2.20)) can also be calculated in saltation in turbulent shearing flows.

Figure 4 shows the variation of the impact angle, the drag coefficient and the particle shear stress at the bed with the particle hold-up, as predicted by ((2.40)–(2.42)), for saltation of 240 μm sand grains in a turbulent wind on Earth, with $\alpha_u = 0.85$ (see § 4 for more details about the choice of the parameters). The range of the hold-ups in figure 4 is that for which (2.23) is satisfied. As for saltation in viscous shearing flows (figure 3), the particle shear stress at the bed increases linearly with M, while θ and C_D are almost constant.

Equation (2.2), with (2.38) and (2.6), and (2.37) can be written as a system of two ordinary differential equations

$$\frac{\mathrm{d}s}{\mathrm{d}y} = -C_D c\frac{\sqrt{r(Sh-s)}}{\kappa}\exp[C_D^2(y+y_0)]Ei[-C_D^2(y+y_0)] - \frac{5}{3}\frac{s}{T_y}; \quad (2.43)$$

and

$$\frac{\mathrm{d}U}{\mathrm{d}y} = \frac{\sqrt{r(Sh-s)}}{\kappa(y+y_0)}; \quad (2.44)$$

these can be numerically integrated, with the boundary conditions of (2.4) and (2.41), to obtain the distributions of the particle shear stress and the fluid horizontal velocity.

Then, the particle horizontal velocity is given by (2.38), with (2.6), as

$$u = U - \frac{\sqrt{r(Sh - s)}}{\kappa} \exp[C_D^2(y + y_0)]Ei[-C_D^2(y + y_0)] - \frac{5}{3}\frac{s}{C_D\sigma_y}. \tag{2.45}$$

Finally, the particle flux q per unit basal area is determined through numerical integration of (2.32), with the profiles of u and c obtained under turbulent conditions.

The above equations permit the determination of profiles of particle concentration, particle and fluid velocities and particle and fluid stresses in turbulent shearing flow that will be compared with the results of DC numerical simulations in § 4.

3. Scaling laws for rarefied saltation

The semi-analytical solutions to particle saltation in shearing flows described in the previous section permit simple asymptotic scalings to be obtained in the limit of rarefied saltation, $M \to 0$ and $s_0 \ll Sh$, and: (i) only Stokes drag, $C_D = 18/St$, that is when the particle Reynolds number based upon the relative velocity between the particles and the fluid at the bed, u_0St/r, is less than unity; or (ii) only form drag, $C_D = 0.3u_0/r$, that is when $10^3 < u_0St/r < 10^5$. In the following, we will consider that at leading order, (2.11) and (2.22) imply that $T_{y,0} \propto h \propto T_{y,0}^{+1/2}/C_D$.

We emphasize that there is no feedback of the particles on the fluid velocity profile, which, in rarefied saltation, is exactly linear in the viscous case, and logarithmic in the turbulent case. As a consequence, the particle hold-up only affects the particle concentration, is linearly proportional to it, and does not influence the particle velocity. Given that the mass flux involves the product of particle concentration and horizontal velocity, q must also be linearly related to the hold-up.

3.1. *Rarefied saltation in viscous shearing flows with Stokes drag*

In this case, the density ratio plays no role in the equations governing the saltation process. As mentioned, $C_D \propto St^{-1}$. Then, with (2.26), we obtain that $\theta \propto St^{-2}Sh^{-1}$. With this, (2.5), (2.15), (2.19) and (2.36) imply the scalings for the various quantities that we report in table 1. In particular, we note that the scaling for the particle flux, $q \propto MSt^4Sh^{3/2}$, was also derived in Valance & Berzi (2022) using an approach in which all particles were assumed to follow the same PT, and not a distribution of trajectories as in the present work.

3.2. *Rarefied saltation in viscous shearing flows with form drag*

In the case of form drag, $C_D \propto u_0 r^{-1}$, and we expect the scaling laws to involve also the density ratio. With (2.5), we obtain $u_0 \propto r^{1/2}\theta^{-1/2}$, and, with (2.26) and (2.15), $\theta \propto r^{-1/3}St^{-2/3}Sh^{-2/3}$ and $T_{y,0}^{+} \propto r$. Hence, (2.5), (2.15), (2.19) and (2.36) imply the scalings for the various quantities that we report in table 1.

3.3. *Rarefied saltation in turbulent shearing flows with Stokes drag*

In this case, $C_D \propto St^{-1}$. At leading order, (2.39) gives $\theta \propto C_D^{-1}r^{-1/2}Sh^{-1/2} \propto r^{-1/2}StSh^{-1/2}$ and (2.15) gives $T_{y,0}^{+} \propto r^{1/2}StSh^{1/2}$. With (2.5), we obtain $u_0 \propto r^{1/2}Sh^{1/2}$, and from (2.21) and (2.22), $h \propto T_{y,0} \propto T_{y,0}^{+1/2}/C_D \propto r^{1/4}St^{3/2}Sh^{1/4}$. Equation (2.19),

	Viscous saltation with Stokes drag	Viscous saltation with form drag	Turbulent saltation with Stokes drag	Turbulent saltation with form drag
Drag coefficient, C_D	St^{-1}	$St^{1/3}Sh^{1/3}r^{-1/3}$	St^{-1}	$Sh^{1/2}r^{-1/2}$
Impact angle, θ	$St^{-2}Sh^{-1}$	$St^{-2/3}Sh^{-2/3}r^{-1/3}$	$StSh^{-1/2}r^{-1/2}$	Sh^{-1}
Particle slip velocity, u_0	St^3Sh	$St^{1/3}Sh^{1/3}r^{2/3}$	$Sh^{1/2}r^{1/2}$	$Sh^{1/2}r^{1/2}$
Depth of saltation layer, h	$St^3Sh^{1/2}$	$St^{-1/3}Sh^{-1/3}r^{5/6}$	$St^{3/2}Sh^{1/4}r^{1/4}$	$Sh^{-1/2}r$
Particle concentration at the bed, c_0	$MSt^{-3}Sh^{-1/2}$	$MSt^{1/3}Sh^{1/3}r^{-5/6}$	$MSt^{-3/2}Sh^{-1/4}r^{-1/4}$	$MSh^{1/2}r^{-1}$
Particle mass flux, q	$MSt^4Sh^{3/2}$	$MSt^{2/3}Sh^{2/3}r^{5/6}$	$MSh^{1/2}r^{1/2}$	$MSh^{1/2}r^{1/2}$

Table 1. Summary of the scaling laws for rarefied saltation.

then, provides $c_0 \propto Mr^{-1/4}St^{-3/2}Sh^{-1/4}$. As shown later, the concentration and particle velocity profiles in the case of turbulent saltation are approximately uniform across the flow. Therefore, we expect $q \propto c_0u_0h \propto Mr^{1/2}Sh^{1/2}$. See the summary of the scalings in table 1.

3.4. *Rarefied saltation in turbulent shearing flows with form drag*

In this limiting case, the fall Stokes number, St, plays no role in the equations governing saltation and cannot be involved in the scalings. With $C_D \propto (\bar{U}-\bar{u})r^{-1}$ and $s_0 = MC_D(\bar{U}-\bar{u})$ with (2.41), we obtain $\bar{U}-\bar{u} \propto r^{1/2}\theta^{-1/2}$, and, with (2.39) and (2.15), at leading order, $\theta \propto C_D^{-1}r^{-1/2}Sh^{-1/2}$ and $T_{y,0}^{+} \propto C_D^{-2}\theta^{-1}$. Hence, $\theta \propto Sh^{-1}$, $T_{y,0}^{+} \propto r$, $u_0 \propto r^{1/2}Sh^{1/2}$, $C_D \propto r^{-1/2}Sh^{1/2}$ and $h \propto T_{y,0} \propto T_{y,0}^{+1/2}/C_D \propto rSh^{-1/2}$. Equation (2.19), then, provides $c_0 \propto Mr^{-1}Sh^{1/2}$. As mentioned, the concentration and particle velocity profiles in the case of turbulent saltation are approximately uniform across the flow. Therefore, we expect $q \propto c_0u_0h \propto MSh^{1/2}r^{1/2}$. We incorporate the scaling laws for rarefied turbulent saltation with form drag in table 1.

4. Comparisons with numerical simulations and experiments

Here, we make comparisons between the predictions of the present theory and the results of DC numerical simulations of saltation of spheres over a rigid bumpy bed made of a layer of particles in close contact. The simulations are performed in a quasi-two-dimensional cell of streamwise length equal to 5120 particle diameters and transverse width equal to one particle diameter, with periodic boundary conditions in the streamwise direction. The cell is not bounded above. We checked that increasing the length in the streamwise direction up to ten times had no effect on the results. Data are available at https://doi.org/10.5281/zenodo.11264272 (Valance 2024).

We solve Newton's equations of motion for the individual spherical particles under the influence of fluid drag, buoyancy, gravity and contact forces in collisions with the bed. Mid-trajectory collisions are forbidden. The fluid is treated as either a viscous or a turbulent flow, depending on the closure for the fluid shear stress, which is governed by a balance equation. The sum over all particles of drag and buoyancy enters the momentum

Description	Regime	St	r	Sh	d_w
60 or 75 μm basalt particles on Mars	viscous (Stokes drag)	60, 100	150 000	0.05, 0.075	1
100 μm basalt particles on Venus	viscous (nonlinear drag)	100	50	0.05	1
650 μm sand particles in water on Earth or, equivalently, 3 mm sand particles in crude oil on Earth	viscous (nonlinear drag)	100	2.5	0.05	1
240 μm sand particles in air on Earth	turbulent (nonlinear drag)	1681	2208	0.025, 0.04	1.5

Table 2. Summary of the combination of parameters employed in the numerical simulations.

balance for the fluid with a change in sign, thus ensuring the two-way coupling between the phases. In the numerical simulations, we assume that the fluid possesses only horizontal velocity and suppress the possibility of interparticle collisions above the bed.

The individual particles experience vertical and horizontal components of fluid drag based upon the local difference between the instantaneous velocity of the particle and the average velocity of the fluid. As in the theoretical treatment, we control the amount of particles in the simulations (the particle hold-up, M); the bumpiness of the rigid bed (the wall-particle diameter, d_w); the fluid viscosity (the inverse of the fall Stokes number, St); the fluid mass density (the inverse of the density ratio, r); and the intensity of the shearing flow (the Shields number, Sh). All measurements have been taken once a steady state is attained and, subsequently, time averaged. Such numerical simulations have already been used in the context of saltation in both turbulent (Durán *et al.* 2012; Pähtz *et al.* 2015; Pähtz & Durán 2020; Ralaiarisoa *et al.* 2020) and viscous (Valance & Berzi 2022) shearing flows. A more detailed description of the numerical simulations, including the contact parameters that we employ, can be found in Appendix D.

In a total of 50 simulations, we have numerically investigated the saltation process of four different types of solid particles in terrestrial and extra-terrestrial environment, as summarized in table 2, by changing the particle hold-up between 0.0004 and approximately 0.0300, that is, from the rarefied limit to the maximum hold-up for which the mid-trajectory collisions can be neglected and (2.23) is satisfied. Although the fluid regime on Mars and Venus is almost certainly turbulent, one can at least imagine performing experiments in pressurized wind tunnels, in which the turbulence is somehow suppressed, thus recovering the conditions reported in the first two rows of table 2. The conditions reported in the last two rows of table 2 are, instead, much closer to actual physical applications.

The flow conditions chosen serve to isolate and test the assumptions that we have made in building the theory: (i) an anisotropic Maxwellian velocity distribution for the particles, the vertical velocity of the ascending particles much larger than the settling velocity and a locally linear velocity for the fluid in the viscous regime, with Stokes drag (the first row in table 2); (ii) the additional assumption of drag coefficient uniform and equal to that evaluated at the bed in the viscous regime, with nonlinear drag (the second and third rows in table 2); and (iii) the fluid velocity profile encountered by ascending particles uniform and equal to the average of the logarithmic profile for the turbulent regime, with nonlinear drag (the fourth row in table 2).

The parameters of the turbulent case in table 2 match those of physical experiments of saltation on rigid, bumpy beds performed in a wind tunnel (Ho 2012). For these, measurements of particle mass flux and profiles of particle concentration and horizontal particle and fluid velocities at different values of the particle hold-up are available.

In the experiments, unlike the numerical simulations, the vertical velocity of the fluid surrounding the particles is non-zero, due to the no-slip condition on the particle surface, and this would permit a test of its influence on the results. However, as shown later, the predicted depth of the saltation layer in the absence of an upper bound and that measured in the numerical simulations is of the order of 4000 particle diameters; while the experiments were performed in a rectangular closed conduit, with a horizontal lid placed at approximately 1200 particle diameters above the rigid base. As a consequence, the top boundary conditions are different from those of the present numerical simulations and the semi-analytical treatment. For this reason, we do not show the profiles of the experiments. Although the order of magnitude of the profiles measured in the experiments is in good agreement with the predictions, their shape reveals the influence of the upper boundary. We postpone to a future work the solution of the appropriate two-point boundary value problem, with our proposed constitutive relations for the particle stresses and energy flux, and detailed comparisons against the experimental measurements.

Figures 5 and 6 show the comparisons between profiles of T_y, c, σ_y, s, u and U relative to selected values of the hold-up for saltation in viscous shearing flows with Stokes drag (the first column of plots in both figures), saltation in viscous shearing flows with nonlinear drag (the second column) and saltation in turbulent shearing flows with nonlinear drag (the third column). A similar agreement between the predictions and the simulations, not shown here for brevity, is obtained for all admissible values of M.

In determining the semi-analytical solution that we have highlighted in § 2, we have employed $\alpha_u = 0.60$ and $\alpha_T = 0.50$ for saltation in viscous flows, and $\alpha_u = 0.85$ and $\alpha_T = 0.18$ for saltation in turbulent flows. We have fitted these values to exactly match the depth of the saltation layer, h, and the particle shear stress at the bed, s_0, in one of the discrete simulations of saltation in viscous flows and one of the simulations of saltation in turbulent flows. Different values of these parameters would not alter the qualitative features of our semi-analytical solution, but impact the values of T_y, c and u at the bed, therefore causing a shift to the right or to the left in the relative profiles. As an overall estimate of their influence, we checked that a ten per cent change in either of the alphas would result in a ten per cent change in the mass flux.

Figures 5(*a*)–5(*c*) confirm that the intensity of the velocity fluctuations of the particles decreases linearly with the distance from the rigid bed, and that the model captures both the weak dependence of T_y on M for viscous saltation and Stokes drag (figure 5*a*), and its independence for nonlinear drag (figures 5*b* and 5*c*). The depth of the saltation layer is well predicted by the continuum model, but the slope of the linear decrease is underestimated with respect to the numerical simulations for nonlinear drag. Also, the non-monotonic behaviour of T_y near the rigid bed is not captured. These are the consequences of neglecting the dependence of the drag coefficient on the vertical direction. The agreement with the measurements in the numerical simulations would indeed improve if C_D is allowed to vary locally; however, this would prevent obtaining semi-analytical solutions of the governing equations, with little improvement on the results. The condition $C_D\sqrt{T_y} > 1$ that ensures that the assumption of large vertical velocities of ascending particles with respect to the settling velocity is sufficiently accurate, is satisfied in the flows of figures 5 and 6 everywhere, but for the upper quarter of the flow, where indeed the deviations between the simulations and the predictions are more significant.

In all cases, the continuum model satisfactorily reproduces the profiles of particle concentration and normal stress in the y-direction (figure 5*d–i*), which indeed follow the power-law distributions of (2.17) and (2.18). In the turbulent case, as anticipated, the particle concentration is rather uniform across the flow (figure 5*f*). The values of

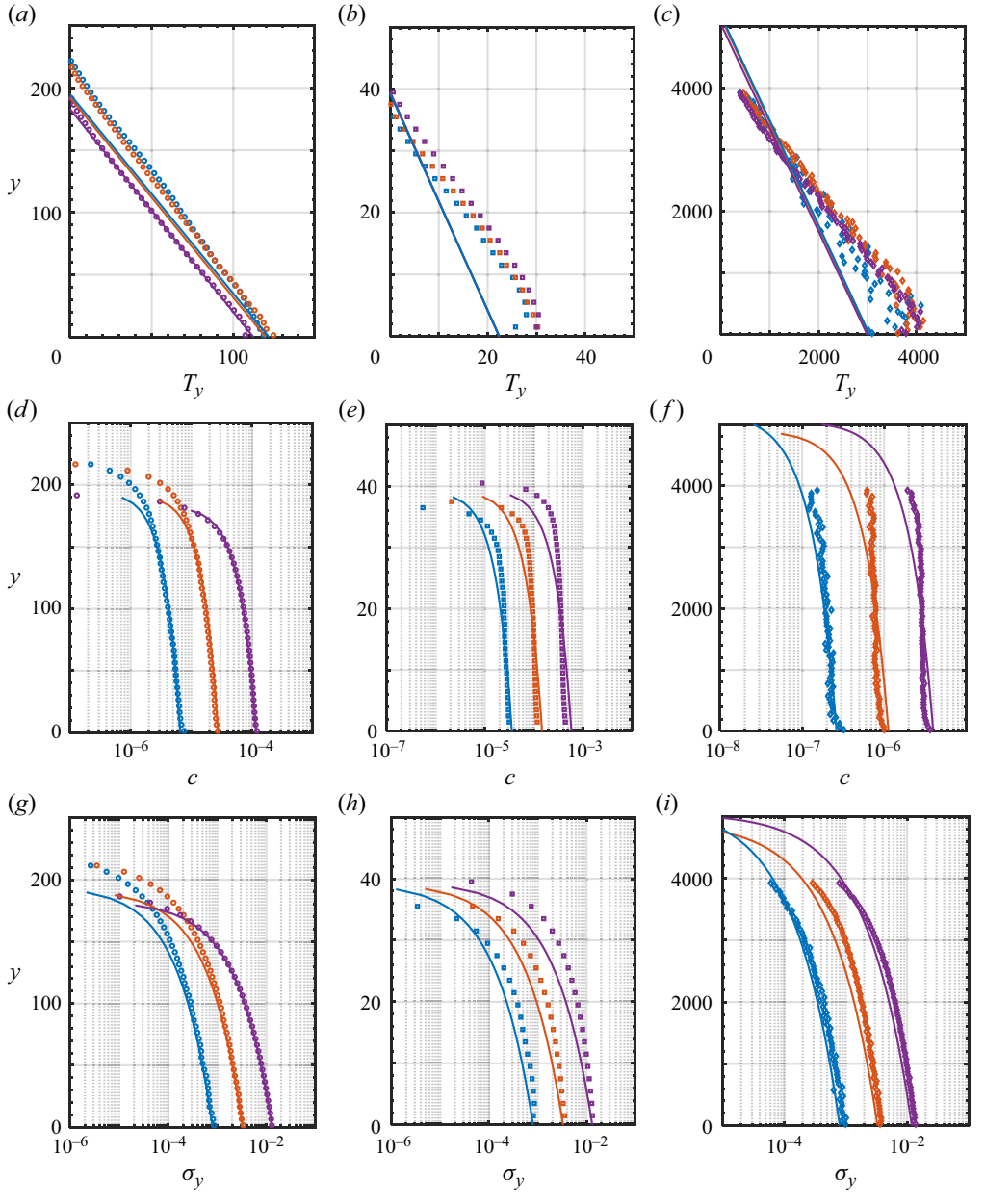

Figure 5. Profiles of (*a–c*) mean square of particle velocity fluctuations in the vertical direction, (*d–f*) particle concentration and (*g–i*) particle normal stress along y measured in numerical simulations of: saltation in viscous shearing flows with $d_w = 1$, $St = 100$, $r = 150\ 000$, $Sh = 0.05$ (first column) and $M = 0.0008$ (blue circles), $M = 0.0033$ (red circles), $M = 0.0131$ (purple circles); saltation in viscous shearing flows with $d_w = 1$, $St = 100$, $r = 50$, $Sh = 0.05$ (second column) and $M = 0.0008$ (blue squares), $M = 0.0033$ (squares), $M = 0.0131$ (purple squares); saltation in turbulent shearing flows with $d_w = 1.5$, $St = 1681$, $r = 2208$, $Sh = 0.04$ (third column) and $M = 0.0008$ (blue diamonds), $M = 0.0033$ (red diamonds), $M = 0.0119$ (purple diamonds). The solid lines are the predictions of the present theory.

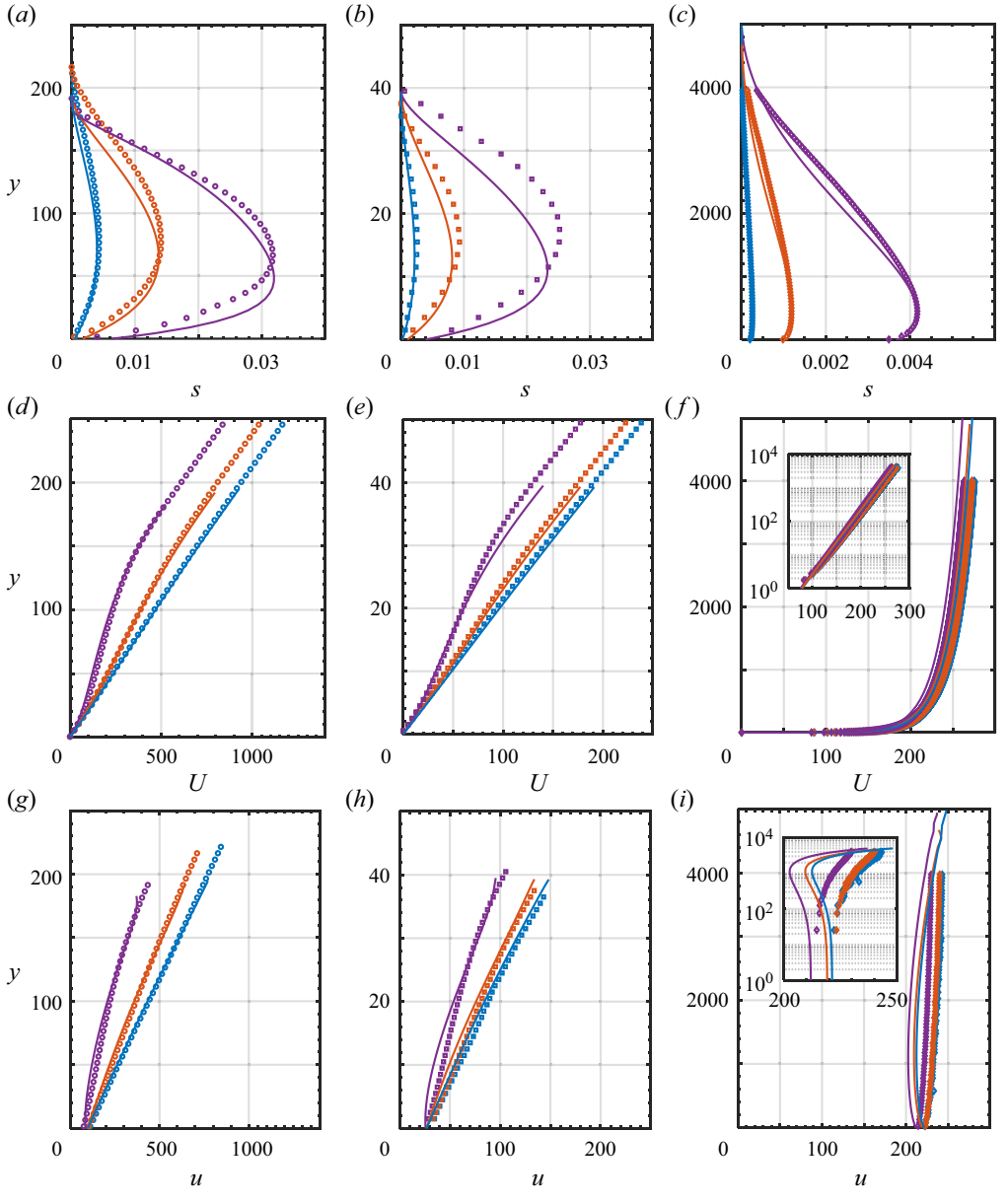

Figure 6. Profiles of (*a–c*) particle shear stress, (*d–f*) fluid and (*g–i*) particle mean horizontal velocities measured in numerical simulations of: saltation in viscous shearing flows with $d_w = 1$, $St = 100$, $r = 150\,000$, $Sh = 0.05$ (first column) and $M = 0.0008$ (blue circles), $M = 0.0033$ (red circles), $M = 0.0131$ (purple circles); saltation in viscous shearing flows with $d_w = 1$, $St = 100$, $r = 50$, $Sh = 0.05$ (second column) and $M = 0.0008$ (blue squares), $M = 0.0033$ (squares), $M = 0.0131$ (purple squares); saltation in turbulent shearing flows with $d_w = 1.5$, $St = 1681$, $r = 2208$, $Sh = 0.04$ (third column) and $M = 0.0008$ (blue diamonds), $M = 0.0033$ (red diamonds), $M = 0.0119$ (purple diamonds). The solid lines are the predictions of the present theory. The insets of figures 6(*f*) and 6(*i*) show the corresponding velocity profiles in semi-log scale.

the particle concentration are also much smaller in the case of turbulent shearing flows (figure 5*f*), as a consequence of the greater agitation of the particles (figure 5*c*).

Figure 5 shows profiles of quantities associated with the vertical motion of the saltating particles, which is sensitive to the horizontal motion of the fluid only through the dependence of the drag coefficient on U. The horizontal motion of the fluid and, in particular, its flow regime, strongly affects the distribution of particle shear stress and particle and fluid horizontal velocity shown in figure 6.

The proposed constitutive relations for the particle shear stress ((2.25) and (2.38)) permit the qualitative and quantitative reproduction of the measurements in numerical simulations (figure 6*a–c*). In particular, the position and the magnitude of the peak in the particle shear stress are well captured. The physical reason for the presence of this maximum value of the particle shear stress above the bed is in the change of sign of the horizontal force exerted by the fluid on the particles. The particles slip at the rigid bed, while the fluid does not; hence, the particles drag the fluid near the bed, while the fluid drags the particles as the top of the saltation layer is approached. Interestingly, the particle shear stress can reach values up to 50 %–60 % of the total shear stress – the Shields parameter – for saltation in viscous shearing flows, but only up to 10 % of the total shear stress for saltation in turbulent shearing flows.

For saltation in viscous shearing flows (Figure 6*d–h*), the fluid and particle horizontal velocity profiles become progressively nonlinear as the particle hold-up increases; but the continuum model is capable of capturing this behaviour. For saltation in turbulent shearing flows, the fluid velocity profile is logarithmic, and the hold-up has little influence on it (figure 6*f*). The horizontal velocity of the particles is almost uniform vertically (figure 6*i*). This confirms our finding that, in the absence of particle interactions, the particle shear stress does not depend on the particle shear rate. The slight discrepancies between the predictions of the continuum model and the results of the numerical simulations are likely due to the assumption of a drag coefficient independent of y.

Finally, we compare the dependence of the particle flux on the particle hold-up in figure 7. The continuum model notably reproduces the measurements in numerical simulations in both the viscous and turbulent shearing flows. The experimental results on turbulent saltation in a wind tunnel (Ho 2012) are in relatively good agreement with both the numerical simulations and the continuum model (figure 7*b*). The overestimate of the experimental mass flux is likely due to the additional resistance induced by the presence of the horizontal lid above the rigid bed. Figure 7(*a*) also assesses the validity of the scaling for q reported in table 1 for the case of viscous saltation and Stokes drag, in the rarefied limit.

5. Conclusions

We have derived constitutive relations for the particle stresses and flux of particle kinetic energy associated with the fluctuating vertical velocities that apply to saltation of particles in viscous and turbulent shearing flows, in the absence of collisions above the bed. To do this, we have employed the averaging methods of statistical mechanics based on an anisotropic Maxwellian velocity distribution function for the ascending particles and approximate analytical expressions for the particle trajectories under the influence of fluid drag, gravity and buoyancy, in the limit of large vertical velocity of ascending particles relative to the settling velocity.

Given that we neglect the possibility of particle–particle interactions, we have obtained the perhaps unexpected result that the particle shear stress does depend on the local relative velocity between the grains and the carried fluid and the fluid shear rate, but not on the

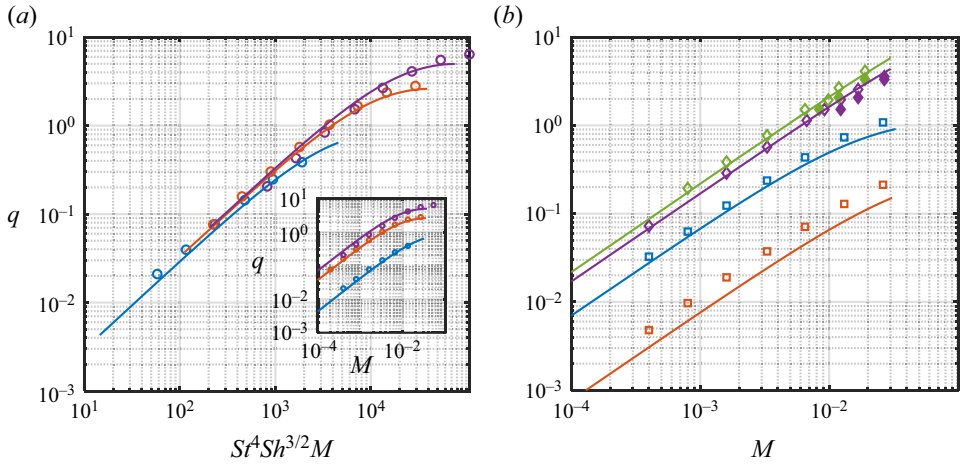

Figure 7. (*a*) Particle flux against scaled particle hold-up measured in DC numerical simulations (open symbols) and predicted from the present theory (lines) in the case of saltation in viscous shearing flows with $d_w = 1$, $r = 150\,000$ and: $St = 60$ and $Sh = 0.05$ (blue circles); $St = 100$ and $Sh = 0.05$ (orange circles); $St = 100$ and $Sh = 0.075$ (purple circles). The inset depicts the same data in terms of q against M. (*b*) Particle flux against particle hold-up measured in DC numerical simulations (open symbols) and in wind-tunnel experiments (filled symbols, after Ho 2012) and predicted from the present theory (lines) in the case of saltation in viscous shearing flows with $d_w = 1$, $St = 100$ $Sh = 0.05$ and $r = 2.5$ (orange squares) and $r = 50$ (blue squares); and in the case of saltation in turbulent shearing flows with $d_w = 1.5$, $St = 1681$, $r = 2208$ and $Sh = 0.025$ (purple diamonds) and $Sh = 0.04$ (green diamonds).

particle shear rate. We have combined the constitutive relations for the particle phase and well-known expressions for the fluid shear stress with momentum and energy balances to obtain semi-analytical solutions of steady, fully developed saltation over horizontal, rigid beds. We have employed boundary conditions appropriated for particles rebounding at a bumpy base with no upper bound to the flow. We have assumed that the carrier fluid has only mean horizontal velocity. Hence, the regime of the carrier fluid, viscous or turbulent, does not affect the profiles of particle concentration and normal stress, which follow a power-law decrease with height, and mean square of the vertical velocity fluctuations, linearly decreasing with the distance from the bed. These results are in contrast with previous theoretical (e.g. Jenkins *et al.* 2010; Jenkins & Valance 2014) and experimental (Creyssels *et al.* 2009) works in which the granular temperature was assumed to be uniform and the concentration was shown to decrease exponentially with height.

We have confirmed our findings through a number of comparisons with DC simulations in both viscous and turbulent regimes. Thus, we are inclined to blame mid-fluid collisions for the above mentioned qualitative difference in the distribution of particle concentration. We have also shown that the predictions of the theory in terms of profiles of particle shear stress, and particle and fluid mean horizontal velocities, are in excellent agreement with the numerical simulations. In natural units of particle mass density, diameter and reduced gravity, we have determined that the saltation process is controlled by the mass of particles in the system, the intensity of the shearing flow, the fluid mass density and viscosity and the bumpiness of the rigid base.

We have successfully tested the dependence of the horizontal particle flux per unit basal area of the particles as a function of the particle hold-up obtained with our theory against DC numerical simulations and wind-tunnel experiments, for a large range of the control parameters. We have also determined simple scaling laws for the dependence of various

quantities of interest on the control variables in the special limits of rarefied viscous and turbulent saltation, and solely Stokes or form drag on the particles.

In a future, we plan to apply our theory to two-point boundary value problems, to e.g. mimic available experiments of saltation in enclosed wind tunnels. We also wish to extend the present work to deal with unsteady and/or developing flows. More importantly, the inclusion of mid-fluid collisions, that is the transition from a collisionless to a collisional kinetic theory of saltation, is a crucial future step, especially in view of modelling transport phenomena over erodible beds, of more interest for geophysical and planetary science applications.

Acknowledgements. We are grateful to T. Pähtz for comments on the manuscript that led to its improvement.

Funding. J.T.J. was supported in part by a Podell Endowment Award for Research and Scholarship from Cornell University. A.V. acknowledges the support of the French Research National Agency through the project ANR-21-CE30–0066.

Declaration of interests. The authors report no conflict of interest.

Author ORCIDs.
Diego Berzi https://orcid.org/0000-0003-0533-2373;
Alexandre Valance https://orcid.org/0000-0001-8076-2192;
James T. Jenkins https://orcid.org/0000-0002-9731-0528.

Appendix A. Approximate analytical trajectories for the saltating particles

We characterize the drag exerted on the particles through a drag coefficient, C_D, that we take to be independent of y, as in Pasini & Jenkins (2005), to obtain analytical expressions for the particle trajectories.

Integrating the vertical momentum balance for the particle

$$\frac{\mathrm{d}\xi_y}{\mathrm{d}t} + C_D\xi_y + 1 = 0, \tag{A1}$$

with ξ_y the vertical component of the particle velocity, we obtain the vertical velocity at any time t after the particle reaches a certain ascending velocity ξ_y^+ at a certain location y_r

$$\xi_y = \frac{C_D\xi_y^+ + 1 - \exp(C_Dt)}{C_D\exp(C_Dt)}; \tag{A2}$$

and, with another integration, the position y as a function of time

$$y - y_r = \frac{(C_D\xi_y^+ + 1)[1 - \exp(-C_Dt)] - C_Dt}{C_D^2}. \tag{A3}$$

From (A3) we obtain an implicit expression for the time that the particle spends at $y \geq y_r$

$$t_f = \frac{C_D\xi_y^+ + 1}{C_D}[1 - \exp(-C_Dt_f)]. \tag{A4}$$

Then, from (A2), with $t = t_f$, the downward vertical velocity of the particle at $y = y_r$ is

$$\xi_y^- = \xi_y^+ - t_f. \tag{A5}$$

To permit subsequent analytical integrations, we propose the following explicit expression for the time of flight

$$t_f = \xi_y^+ + \frac{1}{C_D} - \frac{1}{C_D}\exp(-C_D\xi_y^+), \tag{A6}$$

which has the right limits at both small $C_D\xi_y^+$, i.e. $t_f = 2\xi_y^+$, and large $C_D\xi_y^+$, i.e. $t_f = \xi_y^+ + C_D^{-1}$. With this, (A5) gives

$$\xi_y^- = -\frac{1}{C_D} + \frac{1}{C_D}\exp(-C_D\xi_y^+). \tag{A7}$$

In the limit of large $C_D\xi_y^+$, (A7) reduces to

$$\xi_y^- = -\frac{1}{C_D}. \tag{A8}$$

We next integrate the horizontal particle momentum balances, and distinguish between saltation in viscous and in turbulent shearing flows.

A.1. *Saltation in viscous shearing flows*

In the case of saltation in viscous shearing flows, we assume that the fluid velocity profile is locally linear (that is for $y \geq y_r$), so that the horizontal momentum balance for the particles is

$$\frac{\mathrm{d}\xi_x}{\mathrm{d}t} = C_D\left[U + \frac{\mathrm{d}U}{\mathrm{d}y}(y - y_r) - \xi_x\right], \tag{A9}$$

with ξ_x the horizontal component of the particle velocity, and U and $\mathrm{d}U/\mathrm{d}y$ the fluid horizontal velocity and shear rate at the reference level. In the following integrations, we treat $\mathrm{d}U/\mathrm{d}y$ for saltation in viscous shearing flows as if it were constant. Then, after inserting equation (A3) into (A9), and integrating with the initial condition $\xi_x(t=0) = \xi_x^+$

$$\begin{aligned}\xi_x = U + \frac{\mathrm{d}U}{\mathrm{d}y}\frac{(C_D\xi_y^+ + 1)}{C_D^2}[1 - C_Dt\exp(-C_Dt) - \exp(-C_Dt)] \\ - \frac{\mathrm{d}U}{\mathrm{d}y}\frac{C_Dt - 1 + \exp(-C_Dt)}{C_D^2} + (\xi_x^+ - U)\exp(-C_Dt).\end{aligned} \tag{A10}$$

The horizontal velocity after the time t_f is, then, with (A4) and (A6)

$$\begin{aligned}\xi_x^- = U + \frac{1}{C_D^2}\frac{\mathrm{d}U}{\mathrm{d}y}\frac{1}{C_D\xi_y^+ + 1}[C_D\xi_y^+ + 1 - \exp(-C_D\xi_y^+)][1 - \exp(-C_D\xi_y^+) \\ - C_D\xi_y^+\exp(-C_D\xi_y^+)] + \frac{\xi_x^+ - U}{C_D\xi_y^+ + 1}\exp(-C_D\xi_y^+),\end{aligned} \tag{A11}$$

which in the limit of large $C_D\xi_y^+$ gives

$$\xi_x^- = U + \frac{1}{C_D^2}\frac{\mathrm{d}U}{\mathrm{d}y}. \tag{A12}$$

Equation (A10) can be integrated with the boundary condition $x(t=0) = x_i$ to obtain the horizontal displacement from the initial position at the reference level as a function of

time

$$x = x_i + Ut + \frac{(C_D\xi_y^+ + 1)}{C_D^2}\frac{\mathrm{d}U}{\mathrm{d}y}\left[\exp(-C_Dt)\left(\frac{2}{C_D} + t\right) + t - \frac{2}{C_D}\right] - \frac{1}{C_D^2}\frac{\mathrm{d}U}{\mathrm{d}y}\left[\frac{C_Dt^2}{2} - t - \frac{1}{C_D}\exp(-C_Dt) + \frac{1}{C_D}\right] + \frac{1}{C_D}(\xi_x^+ - U)[1 - \exp(-C_Dt)]. \tag{A13}$$

The horizontal displacement Δ after the time t_f is

$$\Delta = Ut_f + \frac{(C_D\xi_y^+ + 1)}{C_D^2}\frac{\mathrm{d}U}{\mathrm{d}y}\left[\exp(-C_Dt_f)\left(\frac{2}{C_D} + t_f\right) + t_f - \frac{2}{C_D}\right] - \frac{1}{C_D^2}\frac{\mathrm{d}U}{\mathrm{d}y}\left[\frac{C_Dt_f^2}{2} - t_f - \frac{1}{C_D}\exp(-C_Dt_f) + \frac{1}{C_D}\right] + \frac{1}{C_D}(\xi_x^+ - U)[1 - \exp(-C_Dt_f)]. \tag{A14}$$

In the limit of large $C_D\xi_y^+$, $t_f = \xi_y^+ + C_D^{-1}$ and (A14) reduces to

$$\Delta = \frac{1}{2C_D}\frac{\mathrm{d}U}{\mathrm{d}y}\xi_y^{+2} + U\xi_y^+ + \frac{\xi_x^+ - U}{C_D}. \tag{A15}$$

A.2. *Saltation in turbulent shearing flows*

In the case of saltation in turbulent shearing flows, we assume that the fluid velocity above a reference location y_r is the classical logarithmic, $U + \sqrt{rS}\ln[1 + \kappa(\mathrm{d}U/\mathrm{d}y)(y - y_r)/\sqrt{rS}]/\kappa$, obtained by integrating equation (2.44) with the assumption that the fluid shear stress S is independent of y, in which U and $\mathrm{d}U/\mathrm{d}y$ are the fluid horizontal velocity and shear rate at the reference level. Then, the horizontal momentum balance for the particles reads, with (A3)

$$\frac{\mathrm{d}\xi_x}{\mathrm{d}t} = C_DU + C_D\frac{\sqrt{rS}}{\kappa}\ln\left\{1 + \frac{\kappa}{\sqrt{rS}}\frac{(C_D\xi_y^+ + 1)[1 - \exp(-C_Dt)] - C_Dt}{C_D^2}\frac{\mathrm{d}U}{\mathrm{d}y}\right\} - C_D\xi_x. \tag{A16}$$

After integrating equation (A16) with the initial condition $\xi_x(t = 0) = \xi_x^+$

$$\xi_x = \xi_x^+\exp(-C_Dt) + U[1 - \exp(-C_Dt)] + \frac{\sqrt{rS}}{\kappa}\exp(-C_Dt) \times \int_0^{C_Dt}\exp(C_Dt)\ln\left\{1 + \kappa\frac{(C_D\xi_y^+ + 1)[1 - \exp(-C_Dt)] - C_Dt}{C_D^2\sqrt{rS}}\frac{\mathrm{d}U}{\mathrm{d}y}\right\}\mathrm{d}(C_Dt). \tag{A17}$$

The horizontal velocity after the time t_f is, then,

$$\xi_x^- = \xi_x^+\exp(-C_Dt_f) + U[1 - \exp(-C_Dt_f)] + \frac{\sqrt{rS}}{\kappa}\exp(-C_Dt_f) \times \int_0^{C_Dt_f}\exp(C_Dt)\ln\left\{1 + \kappa\frac{(C_D\xi_y^+ + 1)[1 - \exp(-C_Dt)] - C_Dt}{C_D^2\sqrt{rS}}\frac{\mathrm{d}U}{\mathrm{d}y}\right\}\mathrm{d}(C_Dt). \tag{A18}$$

In the limit of large $C_D\xi_y^+$, that is large C_Dt_f, (A18), with (A6), gives the following analytical solution:

$$\xi_x^- = U + \exp(-C_Dt_f)\frac{\sqrt{rS}}{\kappa}\int_0^{C_Dt_f}\exp(C_Dt)\ln\left(1+\frac{C_Dt_f - C_Dt}{C_D^2\frac{\sqrt{rS}}{\kappa}}\frac{\mathrm{d}U}{\mathrm{d}y}\right)\mathrm{d}(C_Dt)$$
$$= U - \frac{\sqrt{rS}}{\kappa}\exp\left[C_D^2\frac{\sqrt{rS}}{\kappa}\left(\frac{\mathrm{d}U}{\mathrm{d}y}\right)^{-1}\right]Ei\left[-C_D^2\frac{\sqrt{rS}}{\kappa}\left(\frac{\mathrm{d}U}{\mathrm{d}y}\right)^{-1}\right], \tag{A19}$$

in which $Ei(x) \equiv -\int_{-x}^{\infty} e^{-t}t^{-1}\,\mathrm{d}t$ is the exponential integral.

Appendix B. Constitutive relations

We define the average of a quantity φ at a certain distance y from the bed as

$$\langle\varphi\rangle = \frac{\pi}{6c}\int_{all\ \xi}\varphi f\,\mathrm{d}^2\boldsymbol{\xi} = \frac{\pi}{6c}\int_{all\ \xi^+}\varphi^+f^+\,\mathrm{d}^2\boldsymbol{\xi}^+ + \frac{\pi}{6c}\int_{all\ \xi^-}\varphi^-f^-\,\mathrm{d}^2\boldsymbol{\xi}^-, \tag{B1}$$

where f is the velocity distribution of particles at that height and $6c/\pi$ is the dimensionless number density. As in Creyssels *et al.* (2009), we distinguish between ascending or descending particles and introduce velocity distributions for both species. We assume that the velocity distribution of the ascending particles is an anisotropic Maxwellian

$$f^+ = \frac{6}{\pi}\frac{c^+}{\pi\sqrt{T_x^+T_y^+}}\exp\left[-\frac{(\xi_x^+ - u)^2}{2T_x^+}\right]\exp\left(-\frac{\xi_y^{+2}}{2T_y^+}\right), \tag{B2}$$

where $u = \langle\xi_x\rangle$ and $T_x^+ = (\pi/6c^+)\int_{all\ \xi^+}(\xi_x^+ - u)^2f^+\,\mathrm{d}^2\boldsymbol{\xi}^+$ and $T_y^+ = (\pi/6c^+)\int_{all\ \xi^+}\xi_y^{+2}f^+\,\mathrm{d}^2\boldsymbol{\xi}^+$ are the mean squares of the horizontal velocity fluctuations of the ascending particles. The concentration of the ascending particles, c^+, is equal to $(\pi/6)\int_{all\ \xi^+}f^+\,\mathrm{d}^2\boldsymbol{\xi}^+$, while that of the descending particle is $c^- = (\pi/6)\int_{all\ \xi^-}f^-\,\mathrm{d}^2\boldsymbol{\xi}^-$. When $\varphi = 1$, (B1) gives $c = c^+ + c^-$.

Given that we are dealing with steady states, $\langle\xi_y\rangle = 0$, so that

$$\langle\xi_y\rangle = \frac{\pi}{6c}\int_{all\ \boldsymbol{\xi}^+}\xi_y^+f^+\,\mathrm{d}^2\boldsymbol{\xi}^+ + \frac{\pi}{6c}\int_{all\ \boldsymbol{\xi}^-}\xi_y^-f^-\,\mathrm{d}^2\boldsymbol{\xi}^- = 0. \tag{B3}$$

Then, we take the limit for large $C_D\xi_y^+$ of ξ_y^- (A9) and, inserting equation (B2) into (B3), and integrating, we obtain

$$c^+C_D\sqrt{\frac{2T_y^+}{\pi}} = c^-. \tag{B4}$$

This is a relation between the concentrations of the two species of particles. As shown later, we find that (B4) does not capture the correct limit as T_y^+ tends to zero, and also slightly underestimates c^-. This is because the limit of large take-off velocity does not capture the fact that the vertical velocity of the descending particles near the top of the saltation layer

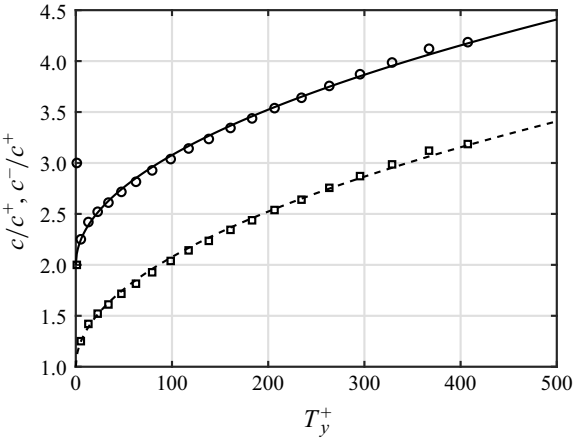

Figure 8. Concentration ratios c/c^+ (circles) and c^-/c^+ (squares) as functions of T_y^+ measured in numerical simulations of saltation in a viscous shearing flow with $d_w = 1$, $St = 100$, $r = 150\ 000$, $Sh = 0.05$ (so that the Stokes drag is dominant and $C_D = 18/St = 0.18$) and $M = 0.0131$. The dashed and solid lines are the predictions of (B5) and (B6), respectively.

is less than the settling velocity. An almost perfect agreement can be obtained, instead, with

$$c^- = c^+ + \frac{3}{4}c^+ C_D\sqrt{\frac{2T_y^+}{\pi}}. \tag{B5}$$

From this and the definition of c

$$c = c^+ + c^- = c^+\left(2 + \frac{3}{4}C_D\sqrt{\frac{2T_y^+}{\pi}}\right). \tag{B6}$$

Taking the limit for large $C_D\xi_y^+$ permits (B4)–(B6) to be obtained without assuming a velocity distribution for the descending particles. We show the comparisons between (B5) and (B6) and the results of numerical simulations on saltation of particles in a viscous shearing flow experiencing Stokes drag in figure 8.

Equation (B1) can be rewritten as

$$\begin{aligned}\langle\varphi\rangle &= \frac{\pi}{6c}\int_{all\ \xi^+}\varphi^+ f^+\,\mathrm{d}^2\boldsymbol{\xi}^+ + \frac{\pi}{6c}\int_{all\ \xi^-}\varphi^- f^-\,\mathrm{d}^2\boldsymbol{\xi}^- \\ &= \frac{\pi}{6c}\int_{all\ \xi^+}\varphi^+ f^+\,\mathrm{d}^2\boldsymbol{\xi}^+ + \frac{\pi}{6c}\int_{all\ \xi^+}\varphi^- f^- |J^-|\,\mathrm{d}^2\boldsymbol{\xi}^+ \\ &= \frac{\pi}{6c}\int_{all\ \xi^+}[\varphi^+ f^+ + \varphi^- f^- |J^-|]\,\mathrm{d}^2\boldsymbol{\xi}^+,\end{aligned} \tag{B7}$$

where J^- is the Jacobian of the transformation from $\boldsymbol{\xi}^+$ into $\boldsymbol{\xi}^-$. When we calculate the average vertical flux of the generic quantity

$$\langle\varphi\xi_y\rangle = \frac{\pi}{6c}\int_{all\ \xi^+}[\varphi^+\xi_y^+f^+ + \varphi^-\boldsymbol{\xi}_y^-f^-|J^-|]\,\mathrm{d}^2\boldsymbol{\xi}^+ = \frac{\pi}{6c}\int_{all\ \xi^+}[\varphi^+ - \varphi^-]\xi_y^+f^+\,\mathrm{d}^2\boldsymbol{\xi}^+, \tag{B8}$$

where we made use of the fact that, at steady state, $\langle\xi_y\rangle = 0$ and, therefore, from (B3), if the trajectories are independent of each other (that is for small particle hold-ups), $\xi_y^+f^+ = -\xi_y^-f^-|J^-|$ (Pasini & Jenkins 2005).

The particle normal stress in the y-direction, in the absence of particle interaction, is simply given by the average vertical flux of y-momentum, $\sigma_y \equiv c\langle\xi_y\xi_y\rangle = cT_y$, where $T_y = \langle\xi_y^2\rangle$ is the mean square of the vertical velocity fluctuation for all the particles. However, using (B8)

$$\sigma_y = \frac{\pi}{6}\int_0^{+\infty}\int_{-\infty}^{+\infty}(\xi_y^+ - \xi_y^-)\xi_y^+f^+\,\mathrm{d}\xi_x^+\,\mathrm{d}\xi_y^+. \tag{B9}$$

Then, upon taking the limit for large $C_D\xi_y^+$ of ξ_y^- (A8) and, inserting equation (B2) into (B9), and integrating, we obtain

$$\begin{aligned}\sigma_y &= \frac{c^+}{\pi\sqrt{T_x^+T_y^+}}\int_0^{+\infty}\left(\xi_y^+ + \frac{1}{C_D}\right)\xi_y^+\exp\left(-\frac{\xi_y^{+2}}{2T_y^+}\right)\int_{-\infty}^{+\infty}\exp\left[-\frac{(\xi_x^+ - u)^2}{2T_x^+}\right]\mathrm{d}\xi_x^+\,\mathrm{d}\xi_y^+\\ &= \frac{c^+}{\pi\sqrt{T_x^+T_y^+}}\sqrt{2\pi T_x^+}\int_0^{+\infty}\left(\xi_y^+ + \frac{1}{C_D}\right)\xi_y^+\exp\left(-\frac{\xi_y^{+2}}{2T_y^+}\right)\mathrm{d}\xi_y^+\\ &= c^+T_y^+ + c^+\frac{1}{C_D}\sqrt{\frac{2T_y^+}{\pi}}.\end{aligned} \tag{B10}$$

The limit for large $C_D\xi_y^+$ permits a simple expression for σ_y (and for the other constitutive relations) to be obtained. This approximation is valid whenever the Maxwellian vertical velocity distribution of the ascending particles is wide, that is for large T_y^+, so that the contribution of the large ξ_y^+ is significant. Conversely, it becomes less accurate near the top of the saltating layer, where we expect small values of T_y^+ and a subsequent narrower distribution of ξ_y^+ around zero. If we use the more accurate equation (A7) in (B9), we would obtain the following constitutive relation for the particle normal stress

$$\begin{aligned}\sigma_y^* &= \frac{c^+}{\pi\sqrt{T_x^+T_y^+}}\int_0^{+\infty}\left(\xi_y^+ + \frac{1}{C_D} - \frac{1}{C_D}\exp(-C_D\xi_y^+)\right)\\ &\quad\times\xi_y^+\exp\left(-\frac{\xi_y^{+2}}{2T_y^+}\right)\int_{-\infty}^{+\infty}\exp\left[-\frac{(\xi_x^+ - u)^2}{2T_x^+}\right]\mathrm{d}\xi_x^+\,\mathrm{d}\xi_y^+\\ &= \frac{c^+}{\pi\sqrt{T_x^+T_y^+}}\sqrt{2\pi T_x^+}\int_0^{+\infty}\left(\xi_y^+ + \frac{1}{C_D} - \frac{1}{C_D}\exp(-C_D\xi_y^+)\right)\xi_y^+\exp\left(-\frac{\xi_y^{+2}}{2T_y^+}\right)\mathrm{d}\xi_y^+\end{aligned}$$

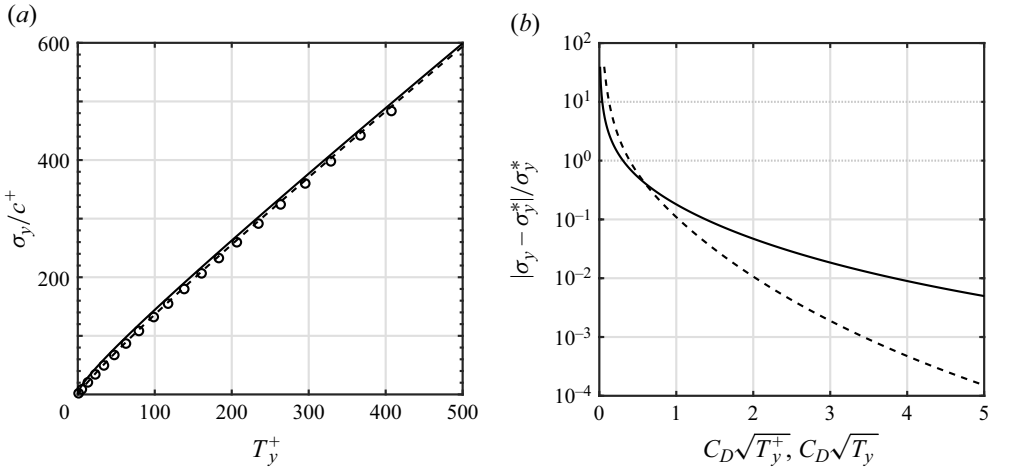

Figure 9. (*a*) Ratio of particle normal stress over particle concentration of ascending particles as a function of T_y^+ measured in numerical simulations of saltation in a viscous shearing flow with $d_w = 1$, $St = 100$, $r = 150\,000$, $Sh = 0.05$ (so that the Stokes drag is dominant and $C_D = 18/St = 0.18$) and $M = 0.0131$. The solid and dashed lines are the predictions of (B10) and (B11), respectively. (*b*) Approximation error on the normal stress as a function of $C_D\sqrt{T_y^+}$ (solid line) and $C_D\sqrt{T_y}$ (dashed line).

$$= c^+T_y^+ + c^+T_y^+ \exp\left(\frac{C_D^2T_y^+}{2}\right) erfc\left(\sqrt{\frac{C_D^2T_y^+}{2}}\right). \tag{B11}$$

The difference between the approximate (B10) and the more accurate (B11) is shown in figure 9(*a*) when the drag coefficient is equal to 0.18. We see that the mismatch becomes relevant only at small T_y^+, as expected. The agreement with the measurements in the numerical simulations of saltation of particles in a viscous shearing flow experiencing Stokes drag is remarkable. Figure 9(*b*) shows the approximation error, $|\sigma_y - \sigma_y^*|/\sigma_y^*$, as a function of $C_D\sqrt{T_y^+}$, that is the ratio of the root-mean-square vertical velocity of ascending particles at a certain position y, $\sqrt{T_y^+}$, over the settling velocity, $1/C_D$.

From $\sigma_y = cT_y$, (B10) and (B6), we obtain

$$T_y = \frac{4\sqrt{\pi}C_DT_y^+ + 4\sqrt{2T_y^+}}{8\sqrt{\pi}C_D + 3C_D^2\sqrt{2T_y^+}}; \tag{B12}$$

while, with (A10),

$$T_y^- = \frac{\pi}{6c^-}\int_{all\ \xi^-}(\xi_y^-)^2 f^-\,\mathrm{d}^2\boldsymbol{\xi}^- = \frac{1}{C_D^2}. \tag{B13}$$

We show the agreement between (B12) and (B13) and the measurements in the numerical simulations of saltation of particles in a viscous shearing flow experiencing Stokes drag in figure 10. Equation (B12) can be employed to plot the approximation error on the normal stress as a function of $C_D\sqrt{T_y}$, that is the ratio of the magnitude of the vertical velocity fluctuations at a certain position y, $\sqrt{T_y}$, over the settling velocity, $1/C_D$ (figure 9*b*). This plot can be used '*a posteriori*' to assess the validity of the large take-off velocity

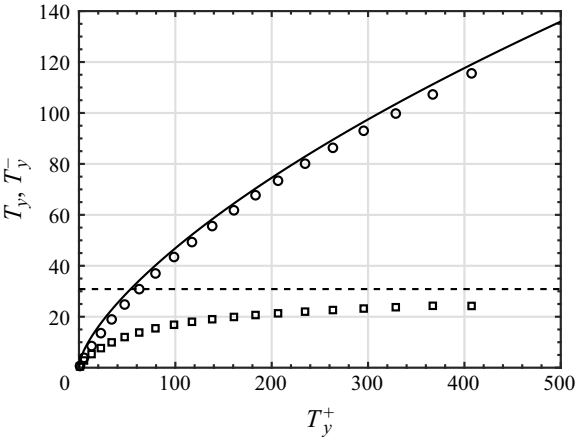

Figure 10. Values of T_y (circles) and T_y^- (squares) as functions of T_y^+ measured in numerical simulations of saltation in a viscous shearing flow $d_w = 1$, $St = 100$, $r = 150\ 000$, $Sh = 0.05$ (so that the Stokes drag is dominant and $C_D = 18/St = 0.18$) and $M = 0.0131$. The solid and dashed lines are the predictions of (B12) and (B13), respectively.

assumption, after the determination of the drag coefficient and the profile of T_y. Figure 9(*b*) indeed shows that the approximation error is less than 10 % for $C_D\sqrt{T_y} > 1$.

The *yyy*-element of the vertical flux of the particle second moment is $Q_{yyy} \equiv c\langle \xi_y \xi_y \xi_y \rangle$, so that, with (B8),

$$Q_{yyy} = \frac{\pi}{6} \int_0^{+\infty} \int_{-\infty}^{+\infty} (\xi_y^{+2} - \xi_y^{-2}) \xi_y^+ f^+ \, \mathrm{d}\xi_x^+ \, \mathrm{d}\xi_y^+. \tag{B14}$$

Then, In the limit of large $C_D\xi_y^+$, upon using (A8) and (B2) in (B14), and integrating

$$\begin{aligned} Q_{yyy} &= \frac{c^+}{\pi\sqrt{T_x^+ T_y^+}} \int_0^{+\infty} \int_{-\infty}^{+\infty} \left(\xi_y^{+2} - \frac{1}{C_D^2}\right) \xi_y^+ \exp\left[-\frac{(\xi_x^+ - u)^2}{2T_x^+}\right] \exp\left(-\frac{\xi_y^{+2}}{2T_y^+}\right) \mathrm{d}\xi_x^+ \, \mathrm{d}\xi_y^+ \\ &= \frac{c^+}{\pi\sqrt{T_x^+ T_y^+}} \sqrt{2\pi T_x^+} \int_0^{+\infty} \xi_y^{+3} \left(1 - \frac{1}{C_D^2 \xi_y^{+2}}\right) \exp\left(-\frac{\xi_y^{+2}}{2T_y^+}\right) \mathrm{d}\xi_y^+ \simeq 2c^+ T_y^+ \sqrt{\frac{2T_y^+}{\pi}}. \end{aligned} \tag{B15}$$

So,

$$Q_{yyy} = \sqrt{\frac{8}{\pi}} c^+ T_y^{+3/2}. \tag{B16}$$

Figure 11 indicates that the prediction of (B16) is in excellent agreement with the measurements in numerical simulations of saltation of particles in a viscous shearing flow experiencing Stokes drag.

The *yy*-element of the dissipation tensor due to fluid drag in the balance of particle second moment is $D_{yy} \equiv 2cC_D\langle \xi_y \xi_y \rangle$ (Saha & Alam 2017), so that, with the definition of

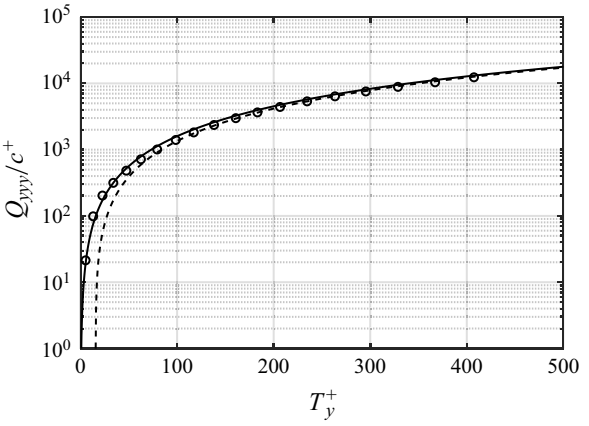

Figure 11. Ratio of energy flux Q_{yyy} over particle concentration of ascending particles as a function of T_y^+ measured in numerical simulations of saltation in a viscous shearing flow with $d_w = 1$, $St = 100$, $r = 150\,000$, $Sh = 0.05$ (so that the Stokes drag is dominant and $C_D = 18/St = 0.18$) and $M = 0.0131$. The solid line is the prediction of (B16).

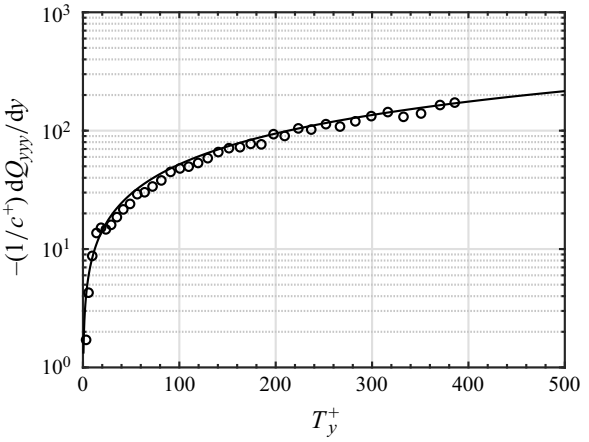

Figure 12. Negative of the derivative of Q_{yyy} over particle concentration of ascending particles as a function of T_y^+ measured in numerical simulations of saltation in a viscous shearing flow with $d_w = 1$, $St = 100$, $r = 150\,000$, $Sh = 0.05$ (so that the Stokes drag is dominant and $C_D = 18/St = 0.18$) and $M = 0.0131$. The solid line is the predictions of D_{yy}/c^+ from (B17).

σ_y and (B10),

$$D_{yy} = 2C_D\sigma_y = 2C_D c^+ T_y^+ + 2c^+\sqrt{\frac{2T_y^+}{\pi}}. \tag{B17}$$

Equation (2.9) indicates that D_{yy} should be equal to the negative of the derivative of Q_{yyy}. Figure 12 shows that the values of $-(1/c^+)\,\mathrm{d}Q_{yyy}/\mathrm{d}y$ measured in numerical simulations of saltation of particles in a viscous shearing flow experiencing Stokes drag as a function of T_y^+ do indeed match the predictions of D_{yy}/c^+ from (B17).

Finally, the particle shear stress is equal to the negative of the average vertical flux of x-momentum, $s \equiv -c\langle \xi_x \xi_y \rangle$, so that, from (B8),

$$s = -\frac{\pi}{6} \int_0^{+\infty} \int_{-\infty}^{+\infty} (\xi_x^+ - \xi_x^-) \xi_y^+ f^+ \, \mathrm{d}\xi_x^+ \, \mathrm{d}\xi_y^+. \tag{B18}$$

To proceed, because of the influence of the fluid velocity on the particle horizontal velocity, we must distinguish between saltation in viscous and turbulent shearing flows.

B.1. *Saltation in viscous shearing flows*

Using (A12) and (B2) into (B18), in the limit of large $C_D \xi_y^+$, and integrating, we obtain the following expression for the particle shear stress:

$$\begin{aligned} s &= -\frac{c^+}{\pi \sqrt{T_x^+ T_y^+}} \int_0^{+\infty} \xi_y^+ \exp\left(-\frac{\xi_y^{+2}}{2T_y^+}\right) \\ &\quad \times \int_{-\infty}^{+\infty} \left[(\xi_x^+ - u) + u - U - \frac{1}{C_D^2} \frac{\mathrm{d}U}{\mathrm{d}y}\right] \exp\left[-\frac{(\xi_x^+ - u)^2}{2T_x^+}\right] \mathrm{d}\xi_x^+ \, \mathrm{d}\xi_y^+ \\ &= \frac{c^+}{\pi \sqrt{T_x^+ T_y^+}} \sqrt{\pi 2 T_x^+} \left(U - u + \frac{1}{C_D^2} \frac{\mathrm{d}U}{\mathrm{d}y}\right) \int_0^{+\infty} \xi_y^+ \exp\left(-\frac{\xi_y^{+2}}{2T_y^+}\right) \mathrm{d}\xi_y^+ \\ &= c^+ \sqrt{\frac{2T_y^+}{\pi}} \left(U - u + \frac{1}{C_D^2} \frac{\mathrm{d}U}{\mathrm{d}y}\right). \end{aligned} \tag{B19}$$

Equation (B19) indicates that there is no influence of T_x^+ on the shear stress, because the assumed Gaussian distribution of ξ_x^+ causes the term involving $(\xi_x^+ - u)$ in the integrand of (B15) to disappear.

However, Valance & Berzi (2022) showed that the probability distribution function of the downward velocity of the particles impacting the bed (dominated by the horizontal component) is actually non-symmetric. Given the perfect agreement with respect to the other constitutive relations obtained in this appendix, which do not involve the horizontal velocity of the ascending particles, we are inclined to ascribe to the non-symmetric distribution of ξ_x^+ the fact that the shear stress measured in simulations of saltation particles in a viscous shearing flow experiencing Stokes drag (figure 13*a*) is not linear in the velocity difference, $U - u$, as implied by (B19).

At small T_y^+, (B10) in (B19) actually indicates that $s \propto C_D \sigma_y (U - u + C_D^{-2} \mathrm{d}U/\mathrm{d}y)$. We found that

$$s = \frac{3}{5} C_D \sigma_y \left(U - u + \frac{2}{3} \frac{1}{C_D^2} \frac{\mathrm{d}U}{\mathrm{d}y}\right), \tag{B20}$$

permits the reproduction of the behaviour of the particle shear stress for saltation in viscous shearing flows with Stokes drag better than (B19) in almost the entire flow domain (figure 13*b*). Although not shown here for brevity, we have assessed that (B20) with the drag coefficient evaluated from the velocity difference at the bed (2.3*a*) works well also in the case of saltation in viscous flows with nonlinear drag.

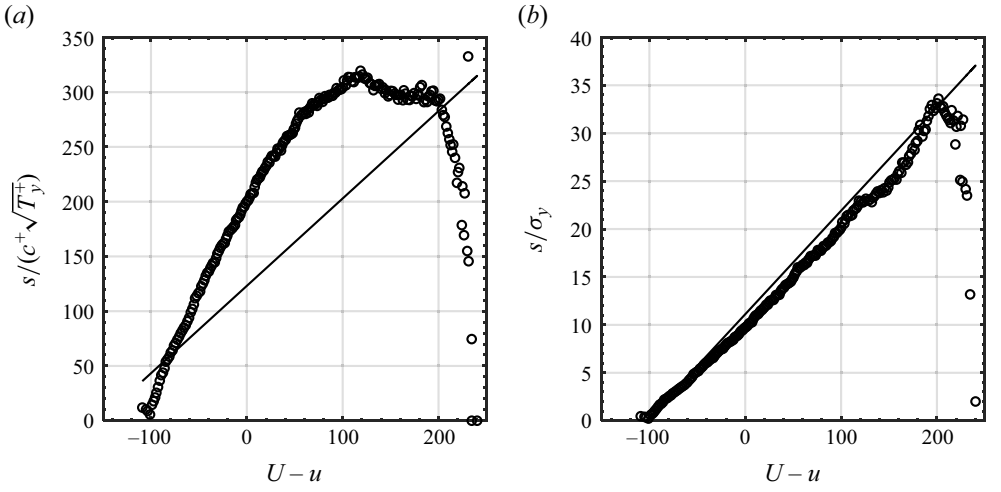

Figure 13. Ratio of (*a*) particle shear stress s and the product of particle concentration of ascending particles and the square root of T_y^+ and (*b*) particle shear stress and the particle normal stress as functions of the velocity difference, $U-u$, measured in numerical simulations of saltation in a viscous shearing flow with $d_w = 1$, $St = 100$, $r = 150\,000$, $Sh = 0.05$ (so that the Stokes drag is dominant and $C_D = 18/St = 0.18$) and $M = 0.0004$. The solid lines are the predictions of (B19) and (B20), respectively.

B.2. *Saltation in turbulent shearing flows*

In the limit of large $C_D\xi_y^+$, using (A19) and (B2) into (B18), and integrating, we obtain the following expression, in the case of saltation in turbulent shearing flows:

$$s = c^+\sqrt{\frac{2T_y^+}{\pi}}\left\{U-u-\frac{\sqrt{rS}}{\kappa}\exp\left[C_D^2\frac{\sqrt{rS}}{\kappa}\left(\frac{\mathrm{d}U}{\mathrm{d}y}\right)^{-1}\right]Ei\left[-C_D^2\frac{\sqrt{rS}}{\kappa}\left(\frac{\mathrm{d}U}{\mathrm{d}y}\right)^{-1}\right]\right\}$$
$$\simeq \frac{3}{5}C_D\sigma_y\left\{U-u-\frac{\sqrt{rS}}{\kappa}\exp\left[C_D^2\frac{\sqrt{rS}}{\kappa}\left(\frac{\mathrm{d}U}{\mathrm{d}y}\right)^{-1}\right]Ei\left[-C_D^2\frac{\sqrt{rS}}{\kappa}\left(\frac{\mathrm{d}U}{\mathrm{d}y}\right)^{-1}\right]\right\}, \tag{B21}$$

where we have kept the same dependency on the drag coefficient and the normal stress as in the case of saltation in viscous shearing flows (B20). In the limit of rarefied saltation, $S \to Sh$, and with (2.37), (B21) becomes

$$\frac{5}{3}\frac{s}{C_D\sigma_y} - U + u = -\frac{2}{3}\frac{\sqrt{rSh}}{\kappa}\exp[C_D^2(y+y_0)]Ei[-C_D^2(y+y_0)]. \tag{B22}$$

The left-hand side of (B22) can be obtained from measurements of s, σ_y, U and u in the numerical simulations and plotted against the vertical position y, to test the validity of the analytical expression on the right-hand side of (B22). If the drag coefficient is evaluated using the concentration-weighted velocity difference (2.3*b*) the agreement is notable (figure 14).

Appendix C. Boundary conditions for shallow impacts at a rigid, bumpy bed

For the case of a single angle of impact θ much less than $\pi/2$ of particles with a large coefficient of friction, so that rolling rather than sliding takes place, the negative of the

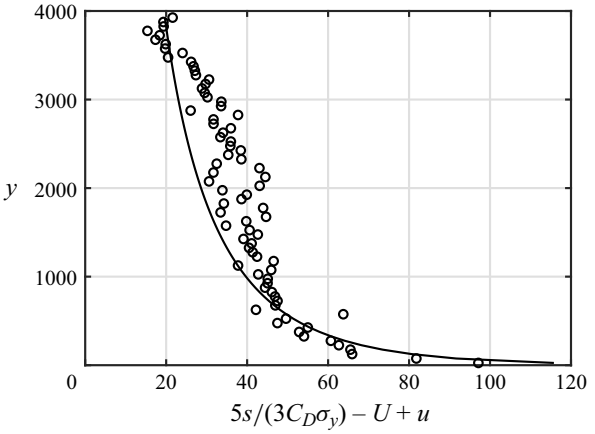

Figure 14. Profile of $5s/(3C_D\sigma_y) - U + u$, with C_D given by (2.3*b*), measured in numerical simulations of saltation in a turbulent shearing flow with $d_w = 1.5$, $St = 1681$, $r = 2208$, $Sh = 0$ and $M = 0.0008$. The solid line is the prediction of (B22).

average ratio of the vertical particle velocity after and before the impact is (Lämmel *et al.* 2017)

$$\left\langle -\frac{\xi_{y,0}^{+}}{\xi_{y,0}^{-}} \right\rangle = -e_t + \frac{2}{3}(e_n + e_t)\sqrt{\frac{2}{\theta}\frac{2d_w}{1+d_w}}, \tag{C1}$$

where e_n and e_t are the coefficients of normal and tangential restitution, respectively, and, here and in what follows, we use the subscript 0 to indicate quantities evaluated at the bed.

For saltation over a rigid, bumpy bed in viscous shearing flows, in the limit of large take-off velocity, (A8), (A12) and (2.24) give

$$\theta = \tan(-\xi_{y,0}^{-}/\xi_{x,0}^{-}) \simeq \frac{C_D}{St(Sh - s_0)}. \tag{C2}$$

In the case of saltation in turbulent shearing flows, instead, in the limit of large take-off velocity, (A8), (A19) and (2.37) give

$$\theta = \tan(-\xi_{y,0}^{-}/\xi_{x,0}^{-}) \simeq -\left[C_D\frac{\sqrt{r(Sh - s_0)}}{\kappa}\exp(C_D^2 y_0)Ei(-C_D^2 y_0)\right]^{-1}. \tag{C3}$$

By inserting (A8) into (C1), we obtain

$$\langle \xi_{y,0}^{+} \rangle = -\frac{e_t}{C_D} + \frac{2\sqrt{2}}{3}(e_n + e_t)\frac{1}{C_D\theta^{1/2}}\sqrt{\frac{2d_w}{1+d_w}}. \tag{C4}$$

Then, we can assume that $T_{y,0}^{+} = \langle (\xi_{y,0}^{+})^2 \rangle \propto \langle \xi_{y,0}^{+} \rangle^2$, so that at leading order,

$$T_{y,0}^{+} = \alpha_T \frac{1}{C_D^2\theta}\frac{2d_w}{1+d_w}, \tag{C5}$$

with the coefficient of proportionality α_T weakly dependent on the coefficients of normal and tangential restitution. Measurements in DC numerical simulations, with θ evaluated as the average angle of impact, shown in figure 15(*a*), confirm the validity of (C5), but

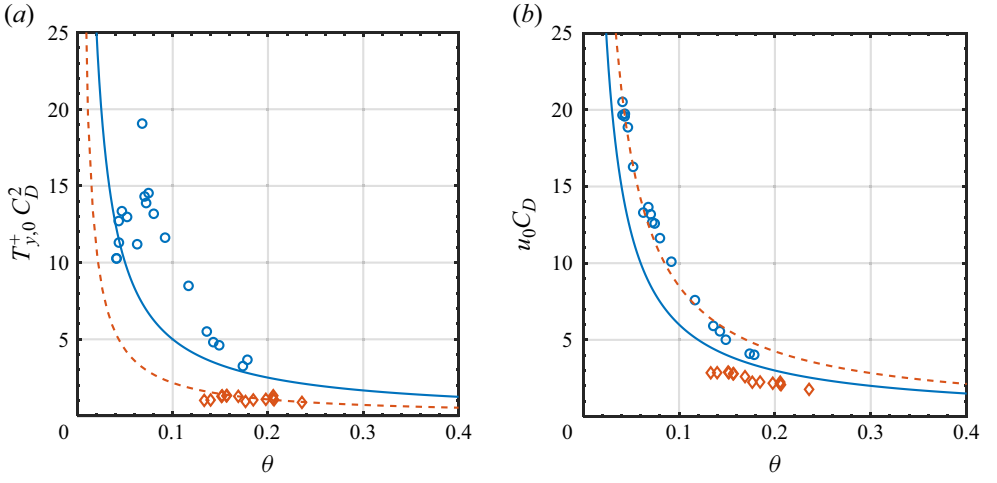

Figure 15. Dependence of (*a*) the mean square of the vertical velocity of ascending particles at the bed and (*b*) the mean horizontal slip velocity on the mean impact angle measured in DC simulations of saltation in viscous (blue circles) and turbulent (orange diamonds) shearing flows. The lines are the predictions of (C5) and (C9), respectively, with: $\alpha_T = 0.50$ and $\alpha_u = 0.60$ (blue solid lines); $\alpha_T = 0.18$ and $\alpha_u = 0.85$ (orange dashed lines). The drag coefficient is evaluated using (2.3*a*) for saltation in viscous flows, and (2.3*b*) for saltation in turbulent flows.

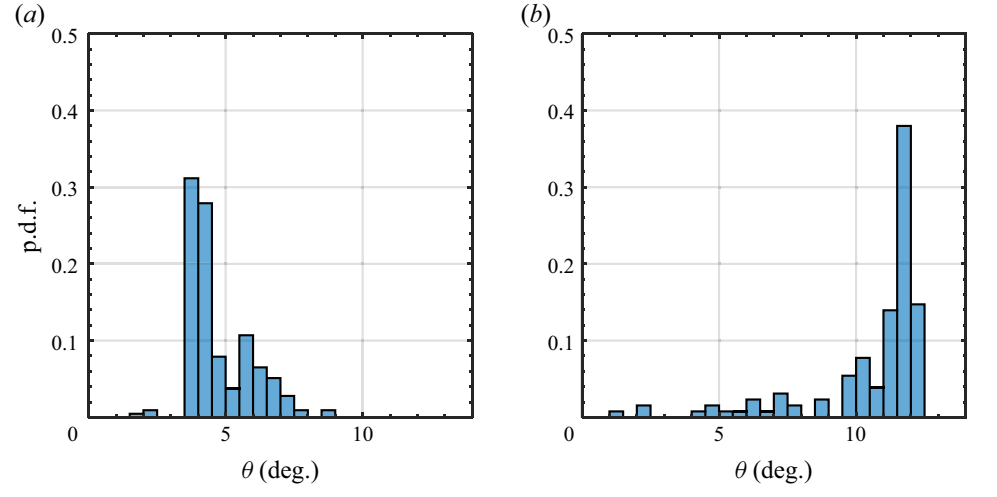

Figure 16. Examples of measured probability distribution function of impact angles in DC simulations of saltation in: (*a*) viscous and (*b*) turbulent shearing flows.

indicate that the coefficient α_T also depends on the flow regime of the fluid. The reason is that the angle of impact is not actually unique: there is a distribution of impact angles of which either (C2) or (C3) provides the most likely value. Measurements in DC simulations (figure 16) reveal that the probability distributions of impact angles for saltation in viscous and turbulent shearing flows are indeed qualitatively different, with a tail respectively to the right or to the left of the peak.

Lämmel *et al.* (2017) also obtained

$$\left\langle \frac{\left(\xi_{y,0}^{+}\right)^2+\left(\xi_{x,0}^{+}\right)^2}{\left(\xi_{y,0}^{-}\right)^2+\left(\xi_{x,0}^{-}\right)^2}\right\rangle = \left[e_t-\frac{(e_t^2-e_n^2)}{2e_t}\theta\frac{2d_w}{1+d_w}\right]^2, \tag{C6}$$

so that, with (A8) and (A12), and $\langle(\xi_{x,0}^{+})^2\rangle \propto \langle\xi_{x,0}^{+}\rangle^2 = \langle u_0^{+}\rangle^2$,

$$u_0^{+} \propto \sqrt{\frac{1}{C_D^2}\left(1+\frac{1}{\theta^2}\right)\left[e_t-\frac{(e_t^2-e_n^2)}{2e_t}\theta\frac{2d_w}{1+d_w}\right]^2 - T_{y,0}^{+}}. \tag{C7}$$

Then, we can determine the total particle slip velocity at the bed as

$$u_0 = \frac{c_0^{+}u_0^{+}+c_0^{-}u_0^{-}}{c_0}. \tag{C8}$$

With (B5) and (B6), and u_0^{-} given by (A12), we obtain, at leading order,

$$u_0 = \alpha_u\frac{1}{C_D\theta}, \tag{C9}$$

where, once again, the coefficient of proportionality α_u is a weak function of the coefficients of restitution and the flow regime of the fluid (figure 15*b*). Using (C5) into (C9) gives

$$u_0 = \frac{\alpha_u}{\alpha_T}\frac{1+d_w}{2d_w}C_D T_{y,0}^{+}. \tag{C10}$$

It is worth mentioning that the values of α_u that we employ do not exactly fit the dependence of the slip velocity on the impact angle (figure 15*b*), but do permit a satisfactory reproduction of the particle shear stress at the bed ((2.28) and (2.41)).

Appendix D. Discrete-continuum numerical simulations

The DC simulation is based on the combination of a DEM for the particle dynamics coupled to a continuum description of hydrodynamics, as developed in Durán *et al.* (2012), Ralaiarisoa *et al.* (2020) and Valance & Berzi (2022).

The particle motion is described by a Lagrangian approach according to which the particle labelled p obeys the following dimensionless equations:

$$\frac{\mathrm{d}\boldsymbol{\xi}^p}{\mathrm{d}t} = -\boldsymbol{e}_y + \sum_q \boldsymbol{f}_c^{p,q} + \boldsymbol{f}_{drag}^{p}, \tag{D1}$$

$$I\frac{\mathrm{d}\boldsymbol{\omega}^p}{\mathrm{d}t} = \frac{1}{2}\sum_q \boldsymbol{n}^{p,q}\times\boldsymbol{f}_c^{p,q}, \tag{D2}$$

where $\boldsymbol{\xi}^p$ and $\boldsymbol{\omega}^p$ are the translational and angular velocity vectors of particle p, respectively; $\boldsymbol{e}_x$ and $\boldsymbol{e}_y$ are the horizontal and vertical unit vectors, respectively; $\boldsymbol{f}_{drag}^{p} = C_D[(U-\xi_x^p)\boldsymbol{e}_x - \xi_y^p\boldsymbol{e}_y]$ is the dimensionless drag force exerted by the fluid on the p-particle and $\boldsymbol{f}_c^{p,q}$ is the dimensionless contact force between particles p and q; $I = 1/10$ is the moment of inertia of a sphere; and $\boldsymbol{n}^{p,q}$ is the unit vector along the contact direction.

The normal component $f_{c,n}$ of the contact force is modelled by a linear spring dashpot, so that $f_{c,n} = (k_n\delta + \gamma_n v_n)$, where k_n is the spring stiffness, δ the overlap between the compliant spheres, γ_n the viscous damping coefficient and v_n the normal component of the relative translational particle velocities. The negative of the ratio between the normal relative velocity before and after the collision is the coefficient of normal restitution e_n. If the values of e_n and k_n are prescribed, γ_n is deduced from the following relation: $\gamma_n = (\pi/6)\sqrt{12k_n/(1+\pi^2/\ln(e_n)^2)}$. The tangential component $f_{c,t}$ of the contact force is described via a Coulomb friction model regularized through a viscous damping: $f_{c,t} = -\min(\mu f_{c,n}, \gamma_t v_t)sign(v_t)$, where μ is the Coulomb friction coefficient, v_t the relative slip velocity at contact and γ_t the tangential viscous damping coefficient. The values chosen for the parameters are: $k_n = \pi/6 \cdot 10^7$, $\gamma_n = \gamma_t$, $e_n = 0.88$ and $\mu = 0.5$.

The fluid motion is solved by an Eulerian description based on (2.24) or (2.37) for viscous and turbulent flows, respectively. The vertical component of the fluid velocity is assumed to be zero, so that only the horizontal momentum balance is required and reads

$$\frac{\mathrm{d}S}{\mathrm{d}y} = F_x, \tag{D3}$$

where $F_x = c\langle\sum_{p\in[y;y+\mathrm{d}y]} C_D(U-\xi_x)\rangle/\langle\sum_{p\in[y;y+\mathrm{d}y]} 1\rangle$, with the angular brackets denoting ensemble averaging, represents the x-component of the average volume force exerted on the fluid by the particles whose centres are located in the horizontal slice between y and $y+\mathrm{d}y$. The integration of (D3) gives

$$S = Sh - \int_0^\infty F_x\,\mathrm{d}y, \tag{D4}$$

where the infinite upper bound of the integral means that all moving grains located above y must be accounted for. Once the vertical profile $S(y)$ of the fluid shear stress is determined, the horizontal fluid velocity profile can then be obtained from the integration equation (2.24) or (2.37) for viscous and turbulent shearing flows, respectively, with the no-slip boundary condition $U = 0$ at $y = 0$.

The simulated system is quasi-two-dimensional with a streamwise length equal to 5120 particle diameters and a transverse length equal to one diameter. We use spherical particles with a polydispersity of $\pm 10\,\%$ and adjust their number in the system to obtain the desired value of the particle hold-up M. Periodic boundary conditions are employed in the streamwise direction. The domain is not upper bounded, while the lower boundary is composed of a layer of immobile particles of diameter d_w in close contact (rigid, bumpy bed; see figure 1). As mentioned earlier in the paper, we suppress the possibility of particle–particle collisions above the bed.

Operatively, at every time step, we integrate equations (D1) and (D2) for every particle in the system and determine its new velocity and position. We then use this information to update the profiles of fluid shear stress and horizontal velocity via (2.4), and (2.24) for viscous flows or (2.37) for turbulent flows and proceed with the next time step until we reach a steady state, that is, when the horizontal mass flux averaged over a window of 100 unit time steps is stationary. Initially, the fluid profile is taken to be linear or logarithmic for viscous and turbulent shearing flows, respectively, and corresponds to the unperturbed profile in the absence of particles. The particles are initially displayed on a horizontal row located at ten diameters from the rigid, bumpy bed, with a constant inter-particle distance equal to two diameters and zero initial velocity. Importantly, the final state is independent of the initial conditions as long as the number of particles in the flow does not surpass its transport capacity.

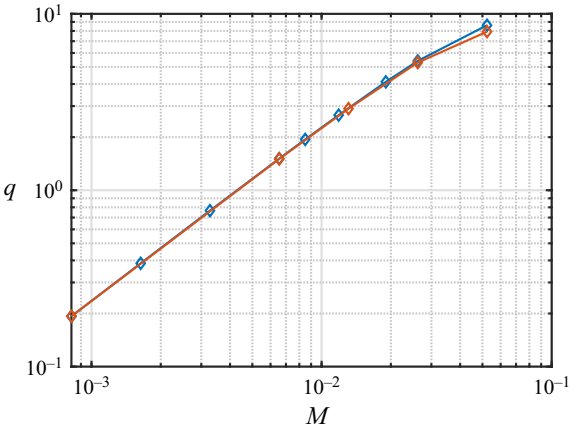

Figure 17. Particle flux against particle hold-up measured in DC numerical simulations with (orange diamonds) and without (blue diamonds) mid-trajectory collisions, in the case of saltation in turbulent shearing flows with $d_w = 1.5$, $St = 1681$, $r = 2208$ and $Sh = 0.04$.

As mentioned, we have suppressed the possibility of mid-trajectory particle–particle interactions in the numerical simulations. However, we have also carried out simulations that incorporate mid-trajectory collisions. As shown in figure 17, such collisions begin to influence the particle flux only for large particle hold-ups, with a concentration that results in a mean free path that does not satisfy the condition of (2.23).

References

Abbott, J.E. & Francis, J.R.D. 1977 Saltation and suspension trajectories of solid grains in a water stream. *Phil. Trans. R. Soc.* A*: Math. Phys. Engng Sci.* **284** (1321), 225–254.

Ancey, C., Bigillon, F., Frey, P., Lanier, J. & Ducret, R. 2002 Saltating motion of a bead in a rapid water stream. *Phys. Rev.* E **66** (3), 036306.

Anderson, R.S., Haff, P.K., Anderson, R.S. & Haff, P.K. 1988 Simulation of eolian saltation. *Science* **241** (4867), 820–823.

Andreotti, B. 2004 A two-species model of aeolian sand transport. *J. Fluid Mech.* **510**, 47–70.

Bagnold, R.A. 1941 *The Physics of Blown Sand and Desert Dunes*. Methuen.

Beladjine, D., Ammi, M., Oger, L. & Valance, A. 2007 Collision process between an incident bead and a three-dimensional granular packing. *Phys. Rev.* E **75** (6), 061305.

Berzi, D., Jenkins, J.T. & Valance, A. 2016 Periodic saltation over hydrodynamically rough beds: aeolian to aquatic. *J. Fluid Mech.* **786**, 190–209.

Berzi, D., Valance, A. & Jenkins, J.T. 2017 The threshold for continuing saltation on Earth and other solar system bodies. *J. Geophys. Res.: Earth Surf.* **122**, 1374–1388.

Burr, D.M., Bridges, N.T., Marshall, J.R., Smith, J.K., White, B.R. & Emery, J.P. 2015 Higher-than-predicted saltation threshold wind speeds on Titan. *Nature* **517**, 60–63.

Chapman, S. & Cowling, T.G. 1970 *The Mathematical Theory of Non-Uniform Gases*, vol. 27. Cambridge University Press.

Charru, F., Andreotti, B. & Claudin, P. 2013 Sand ripples and dunes. *Annu. Rev. Fluid Mech.* **45** (1), 469–493.

Charru, F. & Mouilleron-Arnould, H. 2002 Instability of a bed of particles sheared by a viscous flow. *J. Fluid Mech.* **452**, 303–323.

Chassagne, R., Bonamy, C. & Chauchat, J. 2023 A frictional-collisional model for bedload transport based on kinetic theory of granular flows: discrete and continuum approaches. *J. Fluid Mech.* **964**, 1–39.

Crassous, J., Beladjine, D. & Valance, A. 2007 Impact of a projectile on a granular medium described by a collision model. *Phys. Rev. Lett.* **99** (24), 248001.

CREYSSELS, M., DUPONT, P., OULD EL MOCTAR, A., VALANCE, A., CANTAT, I., JENKINS, J.T., PASINI, J.M. & RASMUSSEN, K.R. 2009 Saltating particles in a turbulent boundary layer: experiment and theory. *J. Fluid Mech.* **625**, 47.

CUNDALL, P.A. & STRACK, O.D.L. 1979 A discrete numerical model for granular assemblies. *Geotechnique* **29** (1), 47–65.

DALL'ACQUA, D., BENUCCI, M., CORVARO, F., LEPORINI, M., COCCI GRIFONI, R., DEL MONACO, A., DI LULLO, A., PASSUCCI, C. & MARCHETTI, B. 2017 Experimental results of pipeline dewatering through surfactant injection. *J. Petrol. Sci. Engng* **159**, 542–552.

DALLAVALLE, J. 1943 *Micromeritics*. Pitman.

DURÁN, O., ANDREOTTI, B. & CLAUDIN, P. 2012 Numerical simulation of turbulent sediment transport, from bed load to saltation. *Phys. Fluids (1994-Present)* **24**, 103306.

FERNANDEZ LUQUE, R. & VAN BEEK, R. 1976 Erosion and transport of bed-load sediment. *J. Hydraul. Res.* **14** (2), 127–144.

GARZÓ, V., TENNETI, S., SUBRAMANIAM, S. & HRENYA, C.M. 2012 Enskog kinetic theory for monodisperse gas-solid flows. *J. Fluid Mech.* **712**, 129–168.

GREELEY, R., IVERSEN, J., LEACH, R., MARSHALL, J., WILLIAMS, S. & WHITE, B. 1984 Windblown sand on venus - preliminary results of laboratory simulations. *Icarus* **57**, 112–124.

GUO, J. & JULIEN, P.Y. 2007 Buffer law and transitional roughness effect in turbulent open-channel flows. In *The Fifth International Symposium on Environmental Hydraulics (ISEH V), Tempe, AZ: University of Nebraska - Lincoln*, 1–6.

HO, T.-D. 2012 Etude expérimentale du transport de particules dans une couche limite turbulente. Université de Rennes 1.

IVERSEN, J.D., POLLACK, J.B., GREELEY, R. & WHITE, B.R. 1976 Saltation threshold on Mars: the effect of interparticle force, surface roughness, and low atmospheric density. *Icarus* **29** (3), 381–393.

IVERSEN, J.D. & WHITE, B.R. 1982 Saltation threshold on Earth, Mars and Venus. *Sedimentology* **29**, 111–119.

JENKINS, J., CANTAT, I. & VALANCE, A. 2010 Continuum model for steady, fully developed saltation above a horizontal particle bed. *Phys. Rev.* E **82**, 020301.

JENKINS, J. & HANES, D. 1998 Collisional sheet flows of sediment driven by a turbulent fluid. *J. Fluid Mech.* **370**, 29–52.

JENKINS, J.T. & VALANCE, A. 2014 Periodic trajectories in aeolian sand transport. *Phys. Fluids* **26** (7), 073301.

JENKINS, J.T. & VALANCE, A. 2018 Two-phase continuum theory for windblown sand. *Phys. Rev. Fluids* **3** (3), 34305.

KOK, J.F., PARTELI, E.J.R., MICHAELS, T.I. & KARAM, D.B. 2012 The physics of wind-blown sand and dust. *Rep. Prog. Phys.* **75** (10), 106901.

KOK, J.F. & RENNO, N.O. 2009 A comprehensive numerical model of steady state saltation (COMSALT). *J. Geophys. Res.: Atmos.* **114** (17), 1–20.

LÄMMEL, M., DZIKOWSKI, K., KROY, K., OGER, L. & VALANCE, A. 2017 Grain-scale modeling and splash parametrization for aeolian sand transport. *Phys. Rev.* E **95** (2), 022902.

LÄMMEL, M., RINGS, D. & KROY, K. 2012 A two-species continuum model for aeolian sand transport. *New J. Phys.* **14**, 093037.

LEPORINI, M., TERENZI, A., MARCHETTI, B., CORVARO, F. & POLONARA, F. 2019 On the numerical simulation of sand transport in liquid and multiphase pipelines. *J. Petrol. Sci. Engng* **175**, 519–535.

NIÑO, Y. & GARCÍA, M. 1998 Experiments on saltation of sand in water. *J. Hydraul. Engng* **124** (10), 1014–1025.

OGER, L., AMMI, M., VALANCE, A. & BELADJINE, D. 2005 Discrete element method studies of the collision of one rapid sphere on 2D and 3D packings. *Eur. Phys. J.* E **17** (4), 467–476.

OURIEMI, M., AUSSILLOUS, P. & GUAZZELLI, É 2009 Sediment dynamics. Part 1. Bed-load transport by laminar shearing flows. *J. Fluid Mech.* **636**, 295.

OWEN, P.R. 1964 Saltation of uniform grains in air. *J. Fluid Mech.* **20** (2), 225–242.

PÄHTZ, T., CLARK, A.H., VALYRAKIS, M. & DURÁN, O. 2020 The physics of sediment transport initiation, cessation, and entrainment across aeolian and fluvial environments. *Rev. Geophys.* **58** (1), e2019RG000679.

PÄHTZ, T. & DURÁN, O. 2020 Unification of aeolian and fluvial sediment transport rate from granular physics. *Phys. Rev. Lett.* **124**, 168001.

PÄHTZ, T., DURÁN, O., HO, T., VALANCE, A. & KOK, J.F. 2015 The fluctuation energy balance in non-suspended fluid-mediated particle transport. *Phys. Fluids* **27**, 013303.

PÄHTZ, T., KOK, J.F. & HERRMANN, H.J. 2012 The apparent roughness of a sand surface blown by wind from an analytical model of saltation. *New J. Phys.* **14**, 043035.

PÄHTZ, T., LIU, Y., XIA, Y., HU, P., HE, Z. & THOLEN, K. 2021 Unified model of sediment transport threshold and rate across weak and intense subaqueous bedload, windblown sand, and windblown snow. *J. Geophys. Res.: Earth Surf.* **126**, e2020JF005859.

PASINI, J.M. & JENKINS, J.T. 2005 Aeolian transport with collisional suspension. *Phil. Trans. Ser.* A *Math. Phys. Engng Sci.* **363** (1832), 1625–1646.

RALAIARISOA, J.L., BESNARD, J.B., FURIERI, B., DUPONT, P., OULD EL MOCTAR, A., NAAIM-BOUVET, F. & VALANCE, A. 2020 Transition from saltation to collisional regime in windblown sand. *Phys. Rev. Lett.* **124** (19), 198501.

SAHA, S. & ALAM, M. 2016 Normal stress differences , their origin and constitutive relations for a sheared granular fluid. *J. Fluid Mech.* **795**, 549–580.

SAHA, S. & ALAM, M. 2017 Revisiting ignited-quenched transition and the non-Newtonian rheology of a sheared dilute gas-solid suspension. *J. Fluid Mech.* **833**, 206–246.

SAUERMANN, G., KROY, K. & HERRMANN, H.J. 2001 A continuum saltation model for sand dunes. *Phys. Rev.* E **64**, 031305.

SEIZILLES, G., LAJEUNESS, E., DEVAUCHELLE, O. & BAK, M. 2014 Cross-stream diffusion in bedload transport. *Phys. Fluids* **26**, 013302.

THOLEN, K., PÄHTZ, T., KAMATH, S., PARTELI, E.J.R. & KROY, K. 2023 Anomalous scaling of aeolian sand transport reveals coupling to bed rheology. *Phys. Rev. Lett.* **130** (5), 58204.

TSUJI, Y., KAWAGUCHI, T. & TANAKA, T. 1993 Discrete particle simulation of two-dimensional fluidized bed. *Powder Technol.* **77** (1), 79–87.

VALANCE, A. 2024 Discrete-Continuum Numerical Simulations of Saltation over a Rigid, Bumpy Bed [Data set]. Zenodo. Available at: https://doi.org/10.5281/zenodo.11264272.

VALANCE, A. & BERZI, D. 2022 Particle saltation over rigid bumpy beds in viscous shearing flows. *J. Fluid Mech.* **947**, 1–28.

VALANCE, A., RASMUSSEN, K.R., OULD EL MOCTAR, A. & DUPONT, P. 2015 The physics of aeolian sand transport. *C. R. Phys.* **16** (1), 105–117.

WERNER, B. 1990 A steady-state model of wind-blown sand transport. *J. Geol.* **98** (1), 1–17.